Modification and Characterization of Alpha and Beta Nickel (II) Hydroxide

Modification and Characterization of Alpha and Beta Nickel (II) Hydroxide

By

Reza Safari

A Thesis Submitted to the Department of Materials Science and Engineering in Partial Fulfillment of the Requirements for the Degree Master of Applied Science

MASTER OF APPLIED SCIENCE (2018) McMaster University

(Materials Science and Engineering) Hamilton, Ontario

TITLE: Modification and Characterization of Alpha and Beta Nickel (II) Hydroxide

AUTHOR: Reza Safari

SUPERVISOR: Professor Gianluigi A. Botton

NUMBER OF PAGES: xii, 81

Abstract

Nickel Hydroxide is one of highly active materials used in various energy conversion applications. One of the key factors in the deposition of $Ni(OH)_2$ is the active surface area which plays an important role in improving the efficiency of transformation reactions. There are various methods to enhance the active area. One method that can be used to modify the morphology of deposited $Ni(OH)_2$ is to generate porous structures. $Ni(OH)_2$ can be formed in two different phases namely alpha and beta. The main objective in our work is to optimize the synthesis conditions and characterize structures at the nanoscale, and also demonstrate unequivocally the presence of alpha and beta phases. For this work, a combination of electron microscopy and electrochemistry is needed to modify the morphology of nickel hydroxide and for detailed structural characterization. Various characterization techniques are used to investigate different electrochemical depositions conditions of $Ni(OH)_2$ in alpha and beta phase forms using Direct and Indirect methods, respectively. Kinetically, α-$Ni(OH)_2$ is easier and faster to be synthesized and can be deposited directly in one step. During cyclic voltammetry of α-$Ni(OH)_2$ in KOH, the volume of material involved in the oxidation reaction increases in every cycle. Scanning Electron Microscopy and Transmission Electron Microscopy characterization shows that this may be due to microbubble formation that transform deposited sheets to particulate shapes. On the other hand, conversion of nickel metal to β-$Ni(OH)_2$ during cyclic voltammetry causes an expansion of particles. Effectively, nickel hydroxide is formed on the shell while nickel remains in the core. High Resolution Transmission Electron Microscopy is then used to identify the distribution of these phases. Another foremost feature for the beta phase is to make nickel metal in any desired shape, which can then be converted to β-$Ni(OH)_2$ through Cyclic Voltammetry in KOH. The presence of both phases is demonstrated with electron diffraction. Finally, as future work, all experiments will be performed in-situ TEM using liquid cell to observe structural changes in real time.

Acknowledgements

First and foremost I would like to thank my supervisor, Dr. Gianluigi Botton for this project and providing best facilities and equipment which are not found easily all around the world. I appreciate his patience, great support and helpful guidance.

I would like to thank Dr. Leyla Soleymani for letting me work in her Lab for electrochemistry experiments. I am forever thankful from Jie Yang for all kinds of support. I also appreciate Carmen Andrei for training me as well as HRTEM tests, Sagar Prabhudev for tomography tests, Chris Butcher for sample preparation, Alex Pofelski and Alfredo Carranco for training the characterization techniques, Travis Casagrande for HRSEM tests, and my best friend, Eric Daigle for all discussions and guidance. I have been lucky and fortunate to be participated in Ni-Electro Can network. This opportunity helped me to collaborate with other universities and institutions. I appreciate Dr. Elena Baranova and her PhD student, Mohamed Houache for providing new samples. Finally, I acknowledge my colleagues and friends for endless help and support.

Table of Contents

List of Figures

List of Abbreviations

2D	Two Dimension
3D	Three Dimension
CA	Chronoamperometry
CE	Counter Electrode
CV	Cyclic Voltammetry
EDS	Energy Dispersive Spectroscopy
ET	Everhart Thornley
FCC	Face-Centre Cubic
FEG	Field Emission Gun
FFT	Fast Fourier Transform
HAADF	High-Angle Annular Dark-field
HCP	Hexagonal Close Packed
HRSEM	High-Resolution Scanning Electron Microscopy
HRTEM	High-Resolution Transmission Electron Microscopy
IFT	Inverse Fourier Transform
PVP	Polyvinylpyrrolidone
RE	Reference Electrode
Redox	Reduction/Oxidation
RGB	Red-Green-Blue
SEM	Scanning Electron Microscopy
TEM	Transmission Electron Microscopy
WE	Working Electrode

1. Introduction

Today, clean energy topics are some of the hottest fields in large-scale research. One of the challenging concerns in the world is the concept of alkaline systems and alkaline batteries (Chen *et al.,* 1999). Nickel is one of the most widely used materials in this field, and Canada and Russia are the most active countries in the world for extraction of nickel resource (Sutherland, 2009). Nickel is an electrochemical active material. Also, nickel is not dangerous such as cadmium and zinc elements regarding toxicity. This material can be used as an energy resource due to specific electronic properties (Chasella & Gatta, 2000). Nowadays, lots of research has been done on this material as well as the energy resources which are using nickel. However, researchers are trying to improve the properties of the material by the combination of chemistry and materials science. In this research, the aim is to improve the properties of Ni-based materials through a better understanding of the microstructure of nickel compounds as well as alkaline reactions involved in energy conversion.

1.1. Alkaline media

The first element which is used in the alkaline battery is nickel and nickel compounds. According to the electrochemistry of materials, nickel hydroxide is a more active and low-cost material with unique electrochemical properties. The alkaline process that causes charging and discharging reactions is displayed in Equations 1.1-1.3 within Figure 1.1. As seen in the alkaline reactions, nickel hydroxide is oxidized

or reacts in the charging reaction. Following this, the water molecule is also reduced, and one free electron is released into the circuit or system. In discharging or return reaction, the electron reduces nickel oxyhydroxide and returns to the stable state (Hutton *et al.,* 2011).

Positive Electrode: $Ni(OH)_2 + OH^- \underset{\text{Discharging}}{\overset{\text{Charging}}{\rightleftharpoons}} NiOOH + H_2O + e^-$ (Eq. 1.1)

Negative Electrode: $M + H_2O + e^- \underset{\text{Discharging}}{\overset{\text{Charging}}{\rightleftharpoons}} MH_{aq} + OH^-$ (Eq. 1.2)

Overall Reaction: $Ni(OH)_2 + M \underset{\text{Discharging}}{\overset{\text{Charging}}{\rightleftharpoons}} NiOOH + MH_{aq}$ (Eq. 1.3)

In general, this reaction is the most important regarding the efficiency of an alkaline system. In other words, the efficiency of a storage system is dependent on this reaction. Every factor that can affect these reactions has an effect on efficiency. There are many approaches to improve an electrochemical reaction. These conditions can be related to the environment, such as temperature, humidity, the purity of materials, reaction speed or charging and discharging rate (Hutton *et al.,* 2011).

1.2. Efficiency of Electrochemical Reactions

The faster oxidation and reduction process in alkaline reactions means more efficiency. The primary condition for the performance of alkaline reactions is the amount of nickel hydroxide. In the first approximation, it is assumed that the amount of nickel hydroxide in a battery or reaction is constant and does not change. Alternatively, electrochemical reactions are carried out uniformly and continuously.

However, at the microscopic scale, nickel hydroxide can be developed and produced on the nanoscale. These reactions are carried out in aqueous solutions, so the solution is expected to be in the vicinity of the solid. The cyclic reactions (charging and discharging) is the due to the presence of the solution or electrolyte in contact with the solid. The more significant the amount of nickel hydroxide in the electrolyte results in the more Redox (Reduction/Oxidation) reactions (Dai *et al.,* 2000). Many approaches are now proposed to enhance the properties of these materials and help with the effectiveness of reactions. One of these approaches is based on structural or morphology changes of the base materials. Porous structures, as well as particle structures, are fundamental to efficient materials. The presence of nano-scale porosities within particles can also help to increase Redox reactions within each particle. Electron microscopy is an effective tool to monitor and detect structural changes in nanomaterials and we therefore focused this study on structural characterization of Ni based nanostructure. In general, the primary goal is to simulate an environment such as an alkaline battery to perform charging and discharging reactions. One method for this simulation is named Droplet method (Sharel *et al.,* 2016). As seen in Fig. 1.2, the working electrode and Pt counter electrode are Positive and Negative poles in an alkaline system, respectively. The Ag/AgCl reference electrode is used to calibrate voltage and current. Finally, the solution plays the same role as the electrolyte in an alkaline battery.

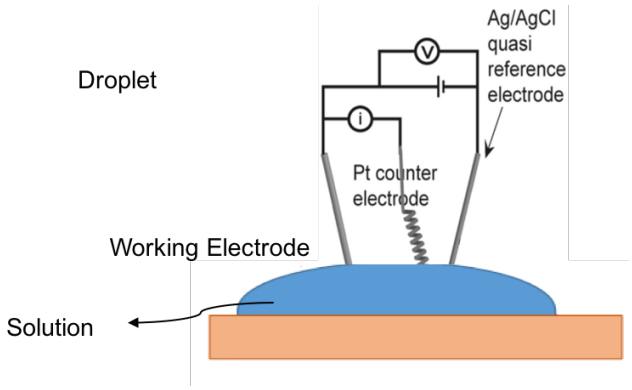

Figure 1.1: The droplet method schematic for simulation of alkaline system, the figure is adapted from (Sharel et al., 2016).

In the next step, depending on the model used, our nickel hydroxide properties are different. Electron microscopy is used to identify these particular properties. Electron Microscopy is one of the world's most powerful characterization tools in the field of material engineering. However, the specific characterization technique that will be used in our work should be introduced first.

1.3. *Ex-situ* Electron Microscopy

In general, methods for characterization of materials are abundant in electron microscopy. In all techniques, such as EDS, Electron Diffraction, Tomography, HRTEM, SEM, etc, the sample needs to be placed in the microscope chamber operated under high vacuum, and the sample normally needs to be prepared under dried and solid form. This is one of the limitations of characterization methods for electrochemical studies. Advanced characterization systems are nowadays designed to study non-solid structures. Usually, these systems are designed so that the sample does

not have direct contact with the column of the microscope. Therefore, no damage occurs to the device and sample. This type of analysis helps to investigate electrochemical reactions usually occurring in aqueous environments, so that structural changes can be observed in the microscope during the reaction. Characterization methods are therefore classified into two general categories. The first concept is based on *in-situ* electron microscopy whereby structural changes are observed during experiments. The second concept is based on *ex-situ* electron microscopy whereby an experiment or a process is carried out outside of the microscope and then observed inside the microscope. However, even though the sample preparation procedure would be easier and compatible with the high vacuum inside of the microscope chamber, there is no longer real-time observation during structural changes (Evans *et al.,* 2011).

1.4. Research Objectives

The objectives of this work are as follows:

1. Synthesis of different forms of nickel hydroxide nanoparticles using electrodeposition procedures to understand Nucleation and Growth mechanism.
2. Modification and fabrication of fine and porous structure of nickel hydroxide which relates to the efficiency of alkaline reactions by higher active surface area.
3. Performing electrochemical reactions such as potential cycling on different shapes of Ni-based materials to investigate the structural changes.
4. Investigation and characterization of nickel hydroxide structures using electron microscopy to demonstrate the presence of the alpha and beta phases.

1.5. Thesis Outline

In this thesis, chapter two reviews the scientific terminology in the field of electrochemistry, the formation of nanoparticles, the setups needed for experiments, and the thermodynamics of electrochemistry. In chapter three, the extraction of information from devices is investigated. The unique properties of synthesized materials, including crystallographic structure, physical and electrochemical properties, are also covered in chapter three. Scientific methods for synthesis as well as special techniques of the electron microscopy used to identify the materials will be described. In the following chapters, the basic sciences of electron microscopy are also briefly mentioned. Finally, using the collected data, the practical steps related to the synthesis of nickel hydroxide nanostructures will be investigated. Therefore, characterization for all stages of synthesis will be provided in detail. Part of the work will involve collaborations with the other research groups who will provide several specimens that are used for experiments.

2. Literature Review

Chapter Outline

The beginning of this chapter examines the concept of simple electrodeposition, Nucleation and Growth concepts. It then covers the methods for characterization of electrochemical reactions such as CA (Chronoamperometry) and CV (Cyclic Voltammetry), and the electrical circuit for the electrochemical reaction. Finally, electrochemical thermodynamics, and how information can be extracted from the CV diagram are explored. In the following, the synthesis of nickel hydroxide based on two different techniques, namely Direct and Indirect, is discussed since these methods lead to two phases: alpha and beta, respectively. In terms of applications, each one of these two phases has its advantages and limitations and, therefore, electron microscopy techniques such as SEM and TEM and their analytical counterparts, namely as electron diffraction, energy dispersive X-ray spectroscopy and electron energy loss spectroscopy, need to be used to analyze the productions of reactions at the nanoscale.

2.1. Electrodeposition of Nanomaterials

Electrodeposition has been widely used in different applications for transformation and modification of materials on the nanoscale. When a voltage is applied between electrodes in a solution, cations which are dissolved into a solution can be reduced on the surface of the working electrode during the electrodeposition process. The reduction reaction is done using an electrical current. These cations can

be stabilized and deposited on the surface of an electrode, the anode, to generate a deposit often with a nanoscale structure (such as a thin film or nanoparticles) (Kissinger & Heineman, 1983). The first step in the deposition process in an electrochemical reaction is the *Nucleation* of nanoparticles. This nucleation is initiated on lower energy sites first in the case of heterogeneous nucleation (Thanh, Maclean & Mahiddine, 2014). For example, pores, grain boundaries and edges of the anode are susceptive to act as nucleation sites. The next step after nucleation is the *Growth* of these nuclei. Depending on the energetics of the growth and interface energy, metal cations might prefer to growth on existing nuclei rather on the low energy sites (Dudin, Unwin & Macpherson, 2010). This results in particle growth. During these two processes, conditions can be controlled by changing the voltage and current in the electrochemical cell so that the morphology of nanostructures can be, in principle, modified. In order to understand the changes in the structure, detailed characterization with microscopy methods is therefore necessary so as to understand how the conditions affect the morphological features and properties.

2.2. Electrochemical Techniques

In an electrochemical reaction, electron movement results in the formation of an electrical circuit. The transport of electrons may cause oxidation and reduction reactions. In order to characterize an electrochemical reaction, a closed environment must be simulated for moving the electrons. Then, using various techniques that control this simulation, instantaneous information can be measured and can be related

to the particular electrochemical reaction. The electrochemical setup and simulation methods are explained below.

2.2.1. Electrochemical Circuit

The setup for an electrochemical reaction is shown in Fig. 2.1. The circuit consists of three electrodes called the working electrode (WE), the reference electrode (RE) and the counter electrode (CE). According to Fig. 2.1, all of these electrodes are connected to a power source. The task of the power source is to generate a current to move reduced ions from within the electrolyte towards an anode where a reaction with electrons from the circuit takes place. The power source generates this current by applying a voltage to the working and counter electrodes. One can then control the voltage and current and record this information as one of the outputs of the experiment (Bard & Faulkner, 1944). The working electrode is an anode where cations are reduced and deposited on it. The counter electrode, the cathode, is a noble metal that does not release a metal ion, but is used to make a connection from the power source to the working electrode through the electrolyte. During the reaction, the voltage of the working electrode changes. These changes are measured relative to the reference electrode voltage. With this geometry in mind, the polarization of the counter electrode does not affect the measured potential for the working electrode (Lertviriyapaisan & Tantavichet, 2010). This configuration has the advantage to provide the absolute potential value, since the Reference electrode has a constant potential. The Reference electrode should be at the closest distance from the Working electrode so that the

solvent resistance does not affect the potential between two electrodes (Lu & Zhao, 2015). With this setup, electrochemical experiments can be done. Two key techniques used to characterize the electrochemical reactions are Chronoamperometry and Cyclic Voltammetry which will be explained below.

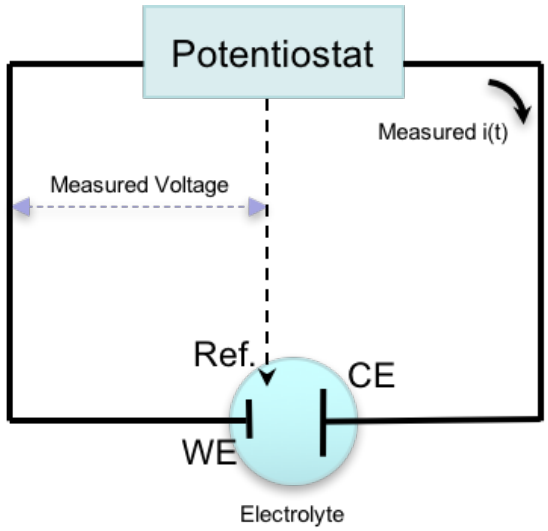

Figure 2.1: Electrochemical circuit including 3 electrodes, the figure adapted from (Bard & Faulkner, 1944).

2.2.2. Chronoamperometry

In the chronoamperometry measurement, a constant voltage between the working electrode and the reference is applied. The length of time during which this voltage is applied depends on how long one desires to observe the electrochemical reaction. When the voltage is applied, the generated current in the circuit is measured. Fig. 2.2 shows the schematic diagram of applied voltage and current response vs. time. This technique is usually used to deposit cations from a solution on the surface of an anode. This voltage is adequate as an activation energy to ionize the cations. Then, the electron is captured by reduction of the cation on the surface, which causes a current

to flow (Denuault, Mirkin & Bard, 1991). Therefore, by measuring this current, the amount of material deposited and condition of deposition are examined.

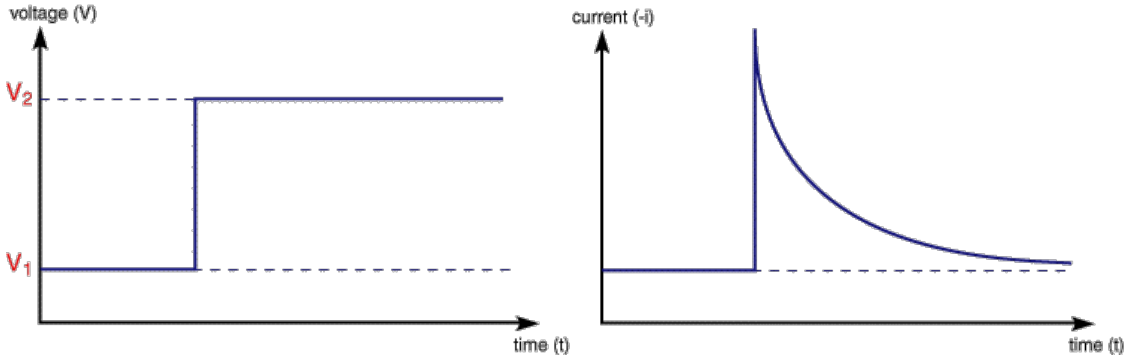

Figure 2.2: Schematic diagram of Chronoamperometry technique, voltage vs. time (Left) and current vs. time (Right) , the figure is from (Fisher, 2010).

2.2.3. Cyclic Voltammetry

In the cyclic voltammetry technique, the voltage increases periodically in a limited time and then decreases at the same rate. This sweeping voltage is considered as one cycle. By increasing and decreasing the voltage over a limited period of time, the current response changes depending on the rate of voltage change. This current flow at the electrodes is measured and used to analyze the reaction (Nicholson, 1965). Fig. 2.3 shows two curves for voltage vs. time and current vs. voltage. This technique is used to perform oxidation and reduction reactions. The deposited material on the surface of the electrode is oxidized at a specific voltage, leading to an increase in the current while the reduction at a different voltage causes a decrease in the current. All these behaviours of current vs voltage help to characterize the Redox reactions.

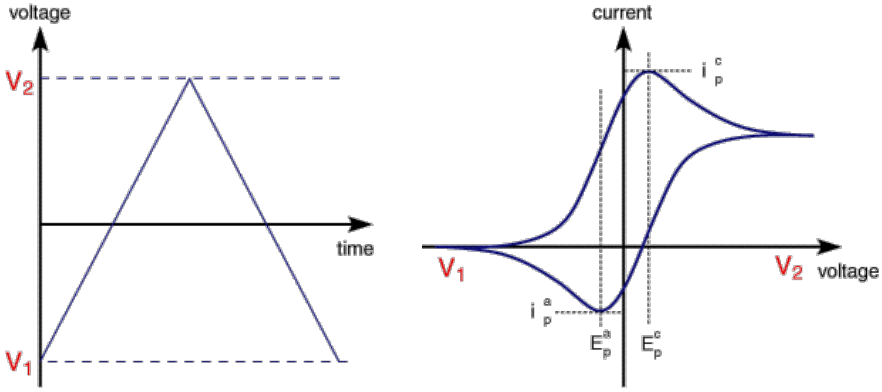

Figure 2.3: Schematic diagrams of Cyclic Voltammetry technique, voltage vs. time (Left) and current vs. voltage (Right) the figure is from (Fisher, 2010).

2.3. Thermodynamic and Electrochemistry

Each one of the previous measurement techniques is used to carry out electrochemical reactions. The principle of these techniques is based on thermodynamics. Thermodynamics theories allow to easily observe the interaction of reactions in the changing conditions of experiments. Also, thermodynamics help to select the test conditions to be optimized. For example, if the final goal is to carry out a cyclic reaction, the range of an oxidation/reduction voltages must be known. Alternatively, for deposition, it would be better to use the thermodynamic calculations to select an optimal voltage and time for this task.

For deposition of metal by a chemical or an electrochemical method, it is first necessary for metal to be transformed to metal ion inside of solution during a reaction. This process requires an energy called Oxidation energy. Heat supplied to the system can provide this energy in a reaction called chemical oxidation or, alternatively electrical energy can be supplied, which generates electrochemical oxidation. In the

previous sections, it was discussed how to make a circuit to apply this energy. By providing a free electron on the anode, these cations can be reduced and returned to their stable metallic state. Therefore, these metals are deposited during an oxidation/reduction evolution from solution onto the anode substrate (Budevski, Staikov & Lorenz, 2000). This process requires energy that is provided from the external power supply. The amount of energy required is obtained from Nernst's equation. If it is assumed that, at any moment, the deposition rate is at a constant rate, this energy is found at a constant temperature. The formula is calculated as follows.

$M \leftrightarrows M^{n+} + ne^-$

$$\Delta G = \Delta G^0 + RT\ln Q \qquad \text{(Eq. 2.1)}$$

Where G is Gibbs free energy and G^0 is the standard state, R is universal gas constant (8.314 $J.K^{-1}.mol^{-1}$), T is temperature and Q is the reaction quotient. The relationship between G and E is as follows.

$$\Delta G = -nFE \qquad \text{(Eq. 2.2)}$$

That n is the number of electrons and F is Faraday constant equal to 9.648×10^4 $C.mol^{-1}$ ($F=N_A q$ that q is the electron charge constant and N_A is Avogadro's number). Therefore, by the combination of Eq. 2.1 and 2.2, Nernst's equation is demonstrated.

$$E_{M/M^{n+}} = E^0_{M/M^{n+}} - \frac{RT}{nF} \ln \frac{a_M}{a_{M^{n+}}} \qquad \text{(Eq. 2.3)}$$

In this equation, a_M and a_M^{n+} are the activities of pure metal and ion, respectively. At room temperature (25 °C), $\frac{RT}{F}$ is equal to 25.69 x 10^{-3} (V). It would be better to use the 10-based logarithm to measure the energy of a cell. Finally, by editing Eq. 2.3 to logarithm and calculation of the constants and swapping the activities, the energy of a cell is quantified by Eq. 2.4 (Budevski, Staikov & Lorenz, 2000).

$$E = E^0 + \frac{0.059\ (V)}{n} log_{10} \frac{a_{Ox.}}{a_{\text{Red.}}} \qquad \text{(Eq. 2.4)}$$

2.4. Characterization of Electrochemical Reactions using CV

As discussed in the previous sections, the current varies by changing the voltage. In both Chronoamperometry and Cyclic Voltammetry tests, the current is measured once with respect to time and once with respect to the voltage, respectively. So, the current curves are needed to characterize a reaction. For example, Fig. 2.4 shows oxidation/reduction of nickel hydroxide. A potentiostat device can measure the current. On another hand, this curve is the result of Eq. 1.1. In this reaction, the nickel hydroxide generates a free electron in the circuit due to oxidation. The oxidation reaction is carried out at a specific voltage in the range of 0.38 to 0.44 volts. As the voltage decreases, the nickel oxyhydroxide is reduced, and the nickel hydroxide becomes stable. At this point, the reduction voltage is between 0.28 to 0.35 volts. Theoretically, if the number of cycles increases in this process, the curve should not show any changes. However, practically, this curve shifts when more cycles are carried

out. Depending on the magnitude and the direction of this shift is, different conclusions can be drawn for the reaction.

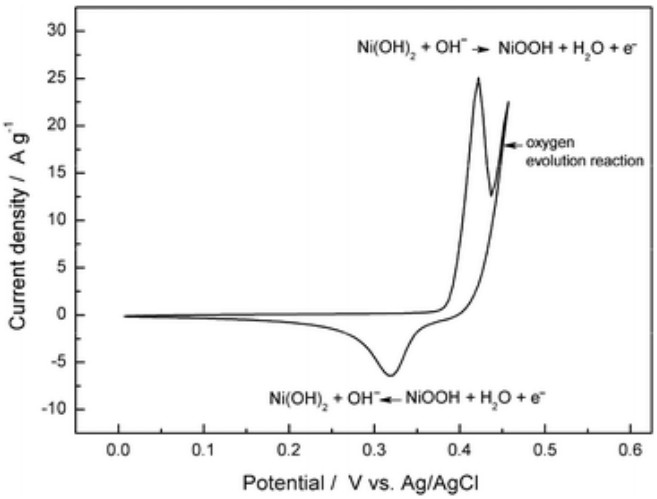

Figure 2.4: Cyclic Voltammetry curve of Nickel Hydroxide, the figure is from (Wu *et al*., 2011).

One of the easiest parameters that can be extracted from this plot is the area under the oxidation peak, which can be used to calculate the amount of active nickel hydroxide (electrode) (Machado & Avaca, 1994). The higher the amount of active surface area results in a larger current. When there are increases or decreases of the area under the oxidation peak, a structural change can be expected. If the shape of the CV diagram changes, this indicates a change of the reaction, and this also indicates that the nanostructure is changing and, as a consequence, the magnitude of the generated current (Alsabet, Grden & Jerkiewics, 2011). For example, Reier et al. 2012 derived that the redox curve of a bulk structure is different from nanoparticle structure. Due to the fine and porous structure of nanoparticles, they exhibit stronger evolution reactions because the electrolyte can easily penetrate through them. As shown in Fig.

2.5, the current of oxidation peak as well as reduction in nanoparticles is approximated 10 times bigger from bulk platinum during CV in 0.1 $MClO_4$.

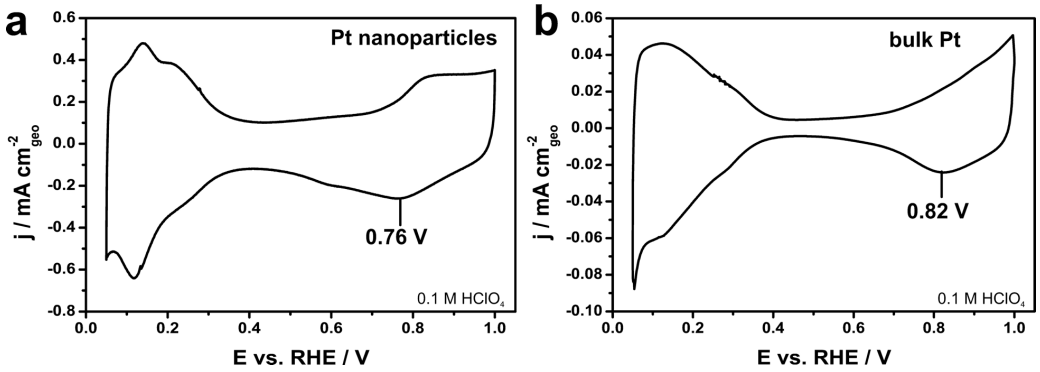

Figure 2.5: Different CV curves of (a) nanoparticles and (b) bulk of Pt, the figure is from (Reier, Oezaslan & Strasser, 2012).

We therefore used the cyclic Voltammetry technique for analyzing and modifying an electrochemical reaction with the help of a potentiostat devices that controls the voltage or/and current in an electrochemical cell.

2.5. Electrochemical and Physical Properties of Nickel Hydroxide

Nickel (II) Hydroxide with $Ni(OH)_2$ formula is an inorganic compound which with significant interest in the field of energy storage. This is one of the low-cost materials with a high electrochemical activity that has been investigated for various applications such as batteries and fuel cells (Zhao *et al*., 2007). This high activity is due to its electrochemical properties. From the electronic point of view, Gong *et al*. 2014 explained that the unpaired electrons of the d shell or empty d orbitals result in an increased propensity for reduction of the nickel hydroxide from an oxidized state

or nickel oxyhydroxide. This property makes nickel hydroxide one of the efficient and high demand materials. One of the applications of nickel hydroxide is as a positive electrode in batteries (Chen *et al*., 1999). As shown previously in Eq. 1.3, the nickel hydroxide is reduced and oxidized by the reaction, which is the same as charging and discharging the battery, respectively. The nickel hydroxide has two polymorphs called alpha and beta (Hall *et al*., 2012). As shown in Fig. 2.6, during the charging and discharging process, the beta-nickel hydroxide is oxidized to the beta-nickel oxyhydroxide. In the case of *Overcharge*, or when high concentration of hydroxide ions or crystalline defects in the beta structure are present, the beta phase is converted into an unstable gamma phase. Oxidation of the alpha phase can also form the gamma phase (Hall *et al*., 2015). In applications for batteries and energy storage, the beta phase is used. From an industrial perspective, the synthesis of the beta phase is more efficient. The alpha phase also has its unique features and properties such as an ageing procedure where the alpha phase can be converted to the beta phase that is desirable (Hu & Noréus, 2003). Therefore, synthesizing each of the two phases has advantages and limitations which will be discussed further below.

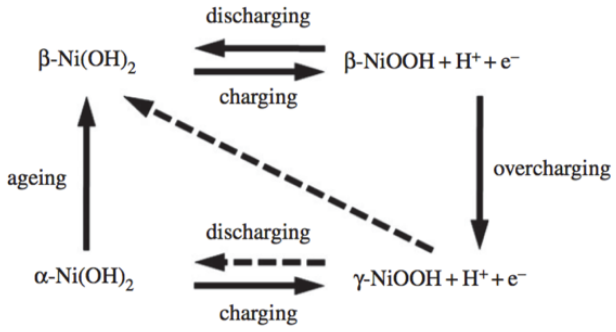

Figure 2.6: Circulation of different phases of Nickel Hydroxide, the figure is from (Hall *et al*., 2015).

2.5.1. Alpha Phase of $Ni(OH)_2$

From the thermodynamic point of view, Rocha et al. 2011 illustrated that the alpha phase is an unstable phase. The crystalline structure of the phase is shown in Fig. 2.7 (a). In this structure, the position of the water molecule lies in a nickel hydroxide layer. Fig. 2.7 (b) highlights the unit cell of alpha-phase. The presence of H_2O layer increases the lattice parameter and decreases the stability of the phase.

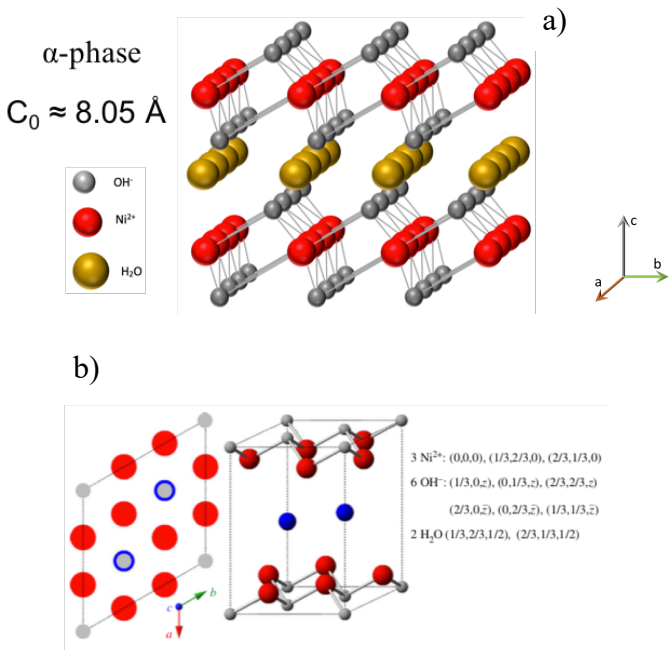

Figure 2.7: Crystalline structure of alpha-nickel hydroxide, a) 3D structure with lattice parameter (Figure adapted from Sharel et al. 2016), b) The unit cell including the atomic positions (Figure from Hall et al., 2015).

The alpha phase lattice parameter is 8.05 Angstrom. This layer is not stable and can be quickly degraded in the electrochemical reactions leading to a change in the structure of the material (Freitas, 2000). Typically, to synthesize this phase, if a high concentration of hydroxide ions is formed on the surface of the electrode in the

presence of the nickel cation, the cation is reduced and deposited on the surface of the substrate. Kinetically, the synthesis of this phase is very fast and easy. This is due to the fact that the hydroxide ion easily forms an ionic bond with the nickel catalysis atoms, which have an empty d orbital and completes the structure. However, this unstable phase needs to be transformed into the beta phase, which requires an ageing process.

2.5.2. Beta Phase of $Ni(OH)_2$

Beta phase of nickel hydroxide is thermodynamically stable (Vidotti *et al.*, 2009). As shown in Fig. 2.8 (a), the structure is close-packed, and the nickel atoms are individually attached to the hydroxide.

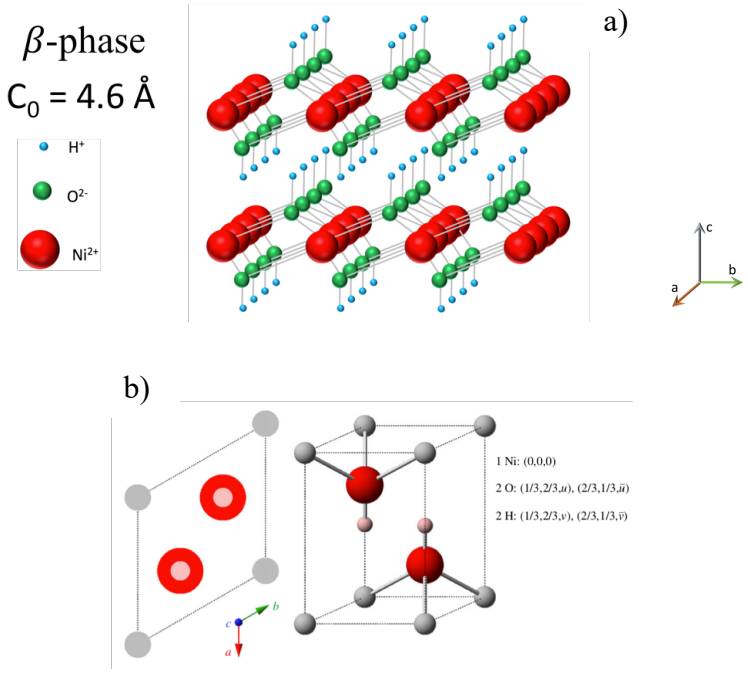

Figure 2.8: Crystalline structure of beta-nickel hydroxide, a) 3D structure with lattice parameter (Figure adapted from Sharel et al. 2016), b) The unit cell including the atomic positions (Figure from Hall et al., 2015).

This is a hexagonal structure with P3m1 space group. The high stability of the beta phase allows the use in electrochemical reactions without changing its crystalline structure. The unit cell and atomic position are also seen in Fig. 2.8 (b). One of the disadvantages of this phase is that the deposition is time-consuming. Usually, this phase is formed in two or more chemical reactions. So, time as well as the difficulties increase.

2.6. Electrodeposition of Nickel (II) Hydroxide

Today, many methods are used for the synthesis of nickel hydroxide nanoparticles in two alpha and beta phases. Mostly, these methods are electrochemical and different structures, depending on synthesis conditions, are obtained. In this research, two principal methods, known as Direct and Indirect methods, proposed by Sharel *et al*., 2016, are discussed. The properties and features of the nanoparticles are very different in two methods, which will be shown in the following chapters.

2.6.1. Direct Approach

In this method, known as the Direct method, using a particular starting compound and electrochemical conditions, the nickel hydroxide is deposited directly and in one step on the surface of a substrate. Based on Eq. 2.5 and Fig. 2.9, the solution containing nickel nitrate ($Ni(NO_3)_2$) is transformed through a reaction with hydroxide ion to nickel hydroxide, and the nitrate ion is released (Sharel et al. 2016).

$$Ni(NO_3)_2 + 2OH^- \rightarrow Ni(OH)_2 + 2NO^-_3 \qquad \text{(Eq. 2.5)}$$

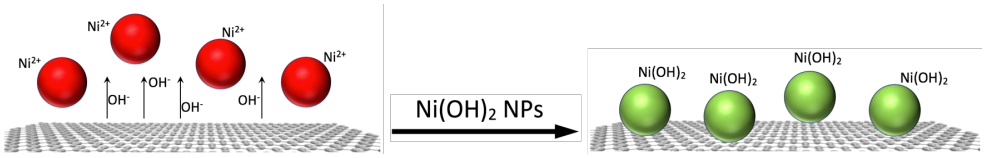

Figure 2.9: One-step processing for deposition of alpha-nickel hydroxide in Direct method, figure adapted from (Sharel et al., 2016).

In this method, the conditions must be adequately controlled, since this reaction depends on the solution concentration, the applied voltage, the surface of a substrate and temperature. The morphology and nanostructure are highly voltage dependent. This reaction is done using chronoamperometry. If longer time is given for the reaction, more nickel hydroxide is produced. One of the challenges in this technique is the thickness of the layer being synthesized. Due to the continuation of the process and formation of a thick layer, the electric current drops; therefore, the layer will not grow uniformly in different regions. Also, due to the different electric fields on the edges and the difference in current density, the structure at the edges is different, non-uniform and uncontrolled.

One of the features of this method is the synthesis of the α-phase. As previously mentioned, the alpha phase is much easier to produce and the synthesis is faster. Sharel *et al*. 2016 also describe that a quick reduction of hydroxide on the surface of the electrode allows nickel to react quickly and provide a layer on a working electrode. To identify the electrochemical reaction, Cyclic Voltammetry can be used to check the quality and electrochemical characteristics of the deposited layer (Eq. 2.6). It should

be noted that the higher number of cycles results in higher nickel hydroxide nanoparticles that are formed, and it is expected that the surface area increases.

$$\alpha\text{-}Ni(OH)_2 + OH^- \leftrightarrows \gamma\text{-}NiOOH^- + H_2O \qquad \text{(Eq. 2.6)}$$

When nickel hydroxide is deposited, the hydroxide ion is needed to perform a cyclic reaction. Therefore, in this case, the electrolyte should be a solution that can quickly be reduced to release the hydroxide ion by changing the voltage. Generally, alkaline solutions would be the best electrolyte. Due to the high activity of these solutions, the hydroxide ion is released generating a higher concentration. The potassium hydroxide and sodium hydroxide are among these solutions used in cyclic reactions. In this reversible reaction (Eq. 2.7), potassium can be easily reduced and then oxidized to return to its active state (Sharel et al. 2016).

$$\alpha\text{-}Ni(OH)_2 + OH^- \rightarrow \gamma\text{-}NiOOH^- + H_2O$$

$$KOH \rightarrow K^+ + OH^-$$

$$\text{---------- (Eq. 2.7)}$$

$$\alpha\text{-}Ni(OH)_2 + KOH \leftrightarrows \gamma\text{-}NiOOH^- + K^+ + H_2O$$

One of the advantages of this method is its speed that can lead to the formation of the nickel hydroxide in a single reaction. The product is also a single-phase structure with no impurities inside of particles. However, in order to reach the useful applications, requiring the β-phase, it is necessary to use an ageing reaction that transform the nickel hydroxide into the beta phase (Sharel et al. 2016).

2.6.2. Indirect Approach

The second method, called Indirect method, is to deposit the beta-nickel hydroxide in two steps. In the first step, nickel metal is deposited on the surface. Indeed, the solution used for this method is different (containing $NiSO_4$), but the synthesis is done in the same way using the chronoamperometry technique. As seen in Eq. 2.8, during an irreversible reaction of an electrode, the nickel is deposited on the surface.

$$2NiSO_4 + 2H_2O \rightarrow 2Ni + 2H_2SO_4 + O_2 \qquad \text{(Eq. 2.8)}$$

In the next step, nickel nanoparticles are converted to nickel hydroxide in an electrochemical reaction. This is done using Cyclic Voltammetry. In this method, according to the following reactions (Eq. 2.9, 2.10), the nickel metal is then converted to β-nickel oxyhydroxide (Fig. 2.10), but in reverse reaction, or reduction of β-$NiOOH^-$, β-nickel hydroxide is formed (Sharel et al. 2016).

$$Ni + 3OH^- \rightarrow \beta\text{-}NiOOH^- + H_2O + 2e^- \qquad \text{(Eq. 2.9)}$$

$$\beta\text{-}NiOOH^- + H_2O \leftrightarrows \beta\text{-}Ni(OH)_2 + OH^- \qquad \text{(Eq. 2.10)}$$

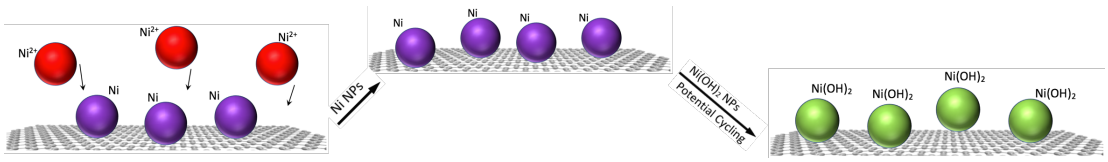

Figure 2.10: Indirect approach for deposition of beta-nickel hydroxide (figure adapted from Sharel et al. 2016).

As one of the advantages of this method, the nickel metal can be converted into nickel hydroxide through a reaction during Cyclic Voltammetry. Therefore, given this approach, it would be easy to synthesize nickel in any shape and form; then, this material can be converted to β-$Ni(OH)_2$. For example, different shapes that have a more active surface area or different particles including porosities would be perfect to use due to the higher oxidation/reduction rate (Sharel et al. 2016).

For the conversion reaction, the solution should be potassium hydroxide which is active enough to release hydroxide ion. The beta phase is synthesized in this method leading to a stable phase, even though the synthesis process is slow. In the conversion reaction, there is always some amount of nickel in the structure. By creating a layer of the nickel hydroxide on the surface, penetration of the hydrogen and oxygen atoms into the structure decreases and the reaction will not occur at the same rate. Therefore, the structure is always double-phases, and there is some remaining nickel in the core of nanoparticles (Sharel et al. 2016).

2.7. Characterization of a Nanostructure using Electron Microscopy Techniques

In this section, the techniques for characterization of materials using electron microscopes are discussed. High magnification is needed for observation of a nanostructure. In the past, optical microscopes were used to analyze materials and to observe microstructures. Due to the limitation of optical lenses, optical microscopes cannot provide a magnification higher than 1000x with an appropriate resolution (Goodhew *et al.,* 2000). This is no longer a limitation for electron microscopes where

the magnification of a good transmission electron microscope can reach up to 10,000,000x. The primary mechanism of these microscopes is that an electron gun accelerates the electron towards a specimen. Also, Goodhew *et al*. 2000 shows that different phenomena occur due to the collision of this electron with the surface of the material. If the specimen thickness is high, the electrons will go inside of the structure, and there will be different phenomena. If the sample is thin enough that an electron can pass through the material, that electron contains the information from the inner structure of a material, such as the crystalline structure information. This is the first classification of electron microscopes. If the electrons provide only surface information and do not get transmitted, the name of this technique is called SEM (Scanning Electron Microscopy), and if the electrons are observed as they pass through the sample, the technique is called TEM (Transmission Electron Microscopy). As the name explains, the electrons are either scanned on the surface or passed through the microstructure, and then the different detectors record different signals. Scanning and bombarding of the sample with electrons in SEM cause generation of secondary electrons. Secondary electrons come from the surface and are either generated from the ejection of inner or outer electron shell of atoms in the sample. By collecting these secondary electrons using an ET (Everhart Thornley) detector, SEM images can be formed. Depending on the voltage of the primary electrons, the penetration of the primary electrons and the origins of the secondary electrons and the quality of images can be substantially different. The voltage in SEM is in the range of a few hundred volts to 40 kV. This voltage would be enough to analyze the sample without damaging

it. In the TEM technique, electrons in the sample are scattered. If a detector is located past the sample, primary electrons, which have been scattered, are recorded in either bright-field or dark-field. This contrast due to scattering (either from diffraction or mass thickness contrast) forms an image in TEM mode. The voltage in TEM can reach to 300 kV. Each technique (either SEM or TEM) techniques have their specific sub-techniques such as energy dispersive spectroscopy or electron energy loss spectroscopy.

2.7.1. Energy Dispersive Spectroscopy (EDS)

This method is based on the characteristic X-ray energy. Inner shell electrons of an atom are excited due to the collision of the primary electrons from the gun in the microscope. In this case, the electrons from an inner shell are ejected. In order to reach a steady state, an electron from outer shells fills the vacant shell. As a result of this electron displacement, X-rays are produced. The difference in energy between two levels of electrons is equal to the energy of the generated X-ray. The energy of this radiation is characteristic for each atom and each of the particular electron shells. So, by measuring the energy of this electron, elemental analysis can be carried out. For example, the iron K_{alpha} shell energy is 6.398 keV, where K is the empty excited orbital, and alpha means an electron from a higher shell, the orbit L, transfers to the empty energy level, and X-ray is generated. Fig. 2.11 is an example of the EDS spectrum of stainless steel. These characteristic energies are fixed for all elements. Finally, the specific detectors can measure these energies separately and show elements and their

weight percent. The EDS techniques can be used in both SEM and TEM (Bruker Nano GmbH, 2015).

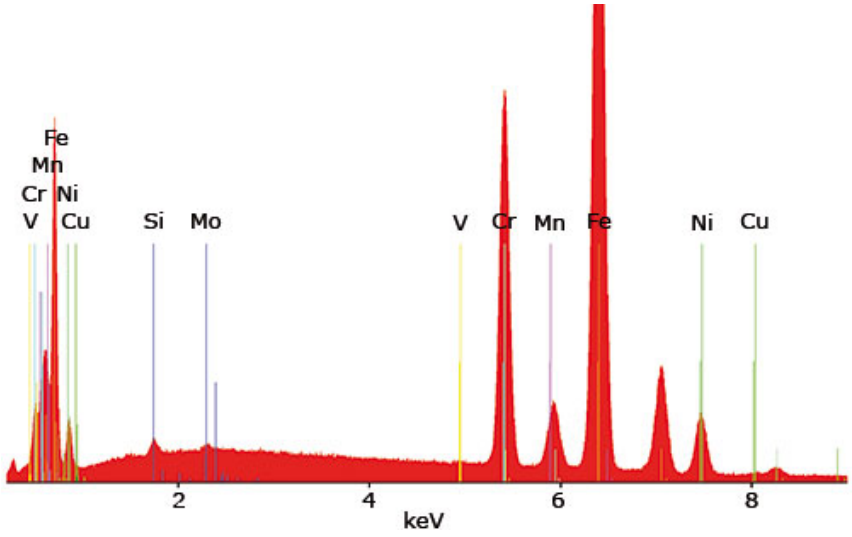

Figure 2.11: The EDS spectrum of a stainless steel, the figure is from (Bruker Nano GmbH, 2015).

2.7.2. High Resolution SEM Analysis (HRSEM)

The high-resolution SEM technique is similar to the SEM with a slight difference in device type and microscope conditions. The lower voltage of the SEM gun results in more details of the surface becoming visible, although the probe size decreases. High-resolution microscopes can be used to magnify 500 kx easily using the field emission source gun with low voltage, special electromagnetic lenses and advanced detectors with better resolution limitation (Roussel *et al.,* 2009). Fig. 2.12 shows the difference between SEM and HRSEM for nickel nanowire where the images show more surface sensitivity for the HRSEM case.

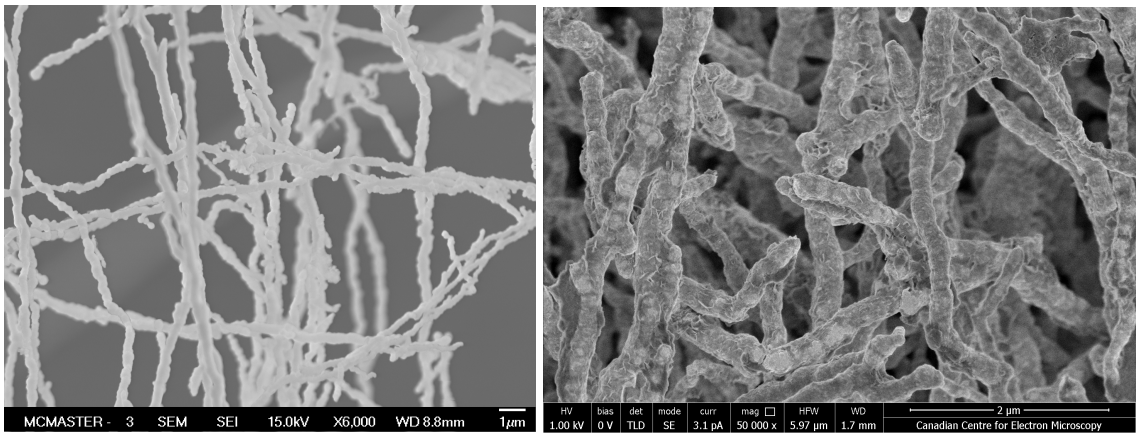

Figure 2.12: Nickel nanowire images, SEM (Left), HRSEM (Right).

2.7.3. Electron Diffraction Analysis in TEM

Another method used to characterize the crystalline structure of various compositions is Electron Diffraction. This technique is commonly used in TEM. When the primary electrons pass through a specimen with a specific crystalline structure, they are diffracted in other direction due to crystalline planes. A group of diffracted beam represents a particular crystalline plane. A total diffraction pattern is obtained from these rays. Any material with a crystalline structure has its diffraction pattern. If the structure is a nanoparticle or polycrystalline, the diffraction pattern is a Ring Pattern. If the specimen is single crystal, the diffraction pattern is a Spot Pattern (Williams & Carter, 1996). The diffraction patterns of the iron compounds, as well as single crystals of α-iron along the zone axis of [-113], is shown in Fig. 2.13.

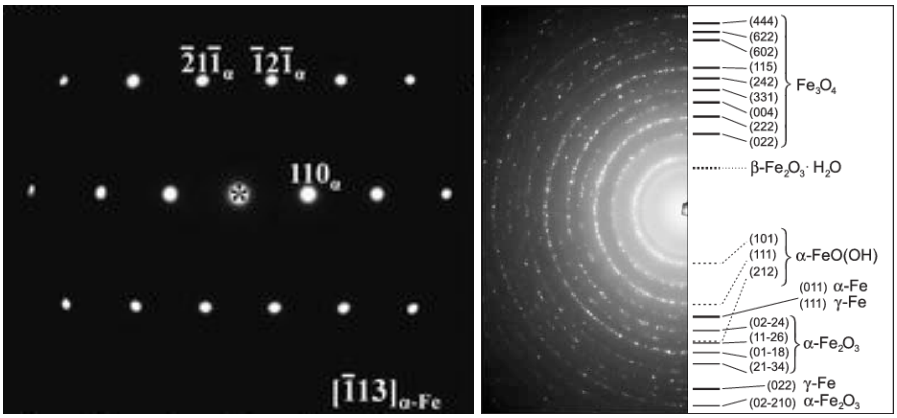

Figure 2.13: The spot pattern of α-Fe (Left), the figure is from (Dehai, 2014) and ring pattern of Fe compounds (Right), the figure is from (Hofmeister et al., 2001).

By measuring the distances between the diffracted spots or lines and the primary beam, the angle of diffraction is calculated. Then with information on the electron wavelengths and scattering angles, the $D_{spacing}$ between the planes is measurable. By comparing these crystalline planes to the database, it is possible to characterize different compounds in a structure.

2.7.4. High Resolution TEM Analysis (HRTEM)

This method is one of the imaging modes of TEM performed on an atomic scale. The mechanism of this method is called Phase Contrast, because of the phase difference between electrons scattered by two (or more) diffracted beams. When the primary beam passes an atom, it is scattered elastically. This scattered beam has a differential phase with the primary beam. By using electron-wave equations and magnetic field functions of lenses, this phase can be calculated. After doing these calculations, high-resolution images can be formed (Gibson, 1991). Fig. 2.14 shows a

high-resolution image of a CeO_2 nanoparticle. With this atomic resolution mode, it is possible to measure the $D_{spacing}$ of atomic planes.

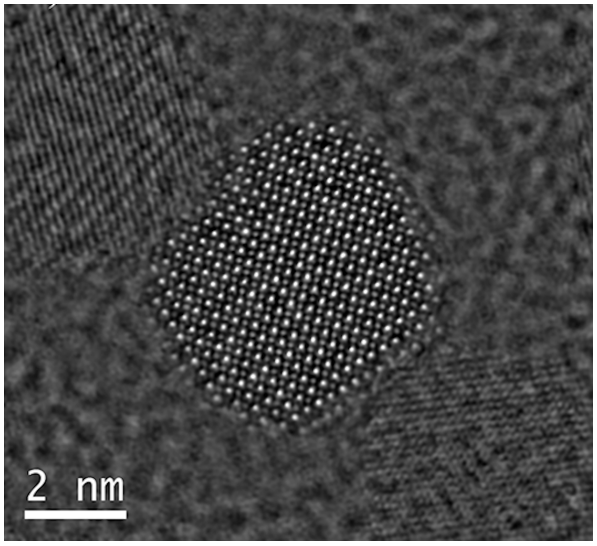

Figure 2.14: HRTEM image of a CeO_2 nanoparticle, the figure is from (Stroppa et al., 2014). This is a phase contrast image in atomic resolution which shows atomic positions. An amorphous phase is placed around particle.

Different phases also can be separated sample using RGB images where each phase identified from diffraction of different planes (unique to each phase) is identified with a basic colour (Red or Green or Blue) so as to more easily identify the spatial distribution of the phases with respect to each other.

2.7.5. Tomography

This method is usually performed in TEM. The purpose of this test is to prepare a three-dimensional (3D) shape of a nanoparticle structure. It is also possible to observe the properties inside of particles. In this method, after loading a sample into a TEM, images are taken at different angles from the sample by rotation of the holder

(Weyland & Midgley, 2004). For example, from the angle of -64 to +64 degrees, a micrograph is taken at every 2 degrees. Due to autofocus, images are not located on a single axis. We have used an image processing software called as TomoJ, for the image processing, including the image alignment. Then, the 3D block of particles is reconstructed. The block is digitally constituted of 2D layers or slices that can show the internal structure of the material in each location. The schematic of this methodology is shown in Fig. 2.15.

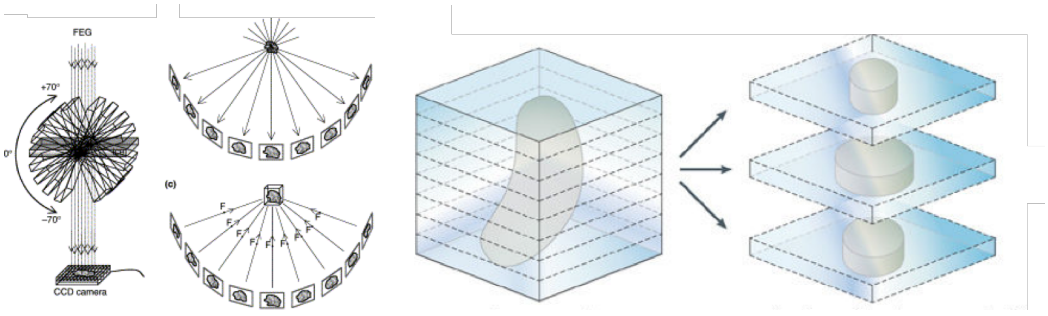

Figure 2.15: Tomography technique using TEM, captured images (Left), the figure is from (Steven & Aebi, 2003), a 3D model of block including slices (Right), the figure is from (Milne & Subramanian, 2009).

2.8. SEM/TEM Limitations

The first limitation of the electron microscopy techniques is sample preparation. In the SEM tests, the specimen becomes charged due to the electron bombardment, and charge trapping if the sample is not conductive. For this reason, SEM samples should always be conductive. In this case, the electrons can be transported out of the sample and to the ground through the holder. This prevents the sample charging. If the sample is charged, the resolution of the image is lost. Also, if there are non-conductive

phases such as polymers, the quality of the image degrades due to contamination. In the TEM test, the sample should be clean. In the presence of impurities and contamination, imaging will be difficult.

There are also limitations in the spectroscopic techniques. In EDS, the X-rays generated must be in high quantities to be sufficiently visible from the background noise. It is therefore usually required to carry out measurements at high voltages and high electron current. However, sometimes the voltage cannot be raised due to the charging of the sample. Also, in the EDS measurements, the weight percent of the elements cannot be accurately measured. Because of the absorption coefficient as well as the fluorescence phenomenon, this measurement requires many corrections that are sometime not accurate depending on the geometry of the sample (Argast *et al*., 2004).

In the HRSEM mode, the alignment is the first limitation. Electromagnetic lenses have astigmatism aberration. Therefore, a distortion in the images is always observed. This limitation is very dependent on the operator of the microscope to remove this aberration.

Analysis of pattern is the main limitation of diffraction. If the sample contains several compounds, the diffraction pattern is very complex and sometimes the various peaks are inseparable. Also, in polycrystalline specimens where crystals are not sufficiently fine, ring patterns will not be formed perfectly and spots patterns are formed from several single crystals. It is therefore challenging to distinguish these phases.

In the HRTEM method, the sample must be stable. Also, due to the high magnification of these images, there should not be any vibration. In addition, these images are created only in places where the sample thickness is very low. Otherwise, the atomic resolution is reduced, and the images include several orientations (Buseck, Cowley & Eyring, 1988).

The Image processing software is also significant limitation in Tomography tests. To align images on a single axis, the number of images at different angles is vital; consequently, that is time-consuming. A large number of images makes the 3D model more accurate (Aert *et al.,* 2011). Another limitation is the holder rotation. The particles that are chosen should be placed in the middle of the TEM grid to be visible even at high angles.

3. Experimental Methods

3.1. Electrodeposition Setup

In this research, different materials have been used to provide a suitable substrate for deposition of nickel hydroxide. One of the essential substrates is wrinkled gold. Fig. 3.1 shows the SEM image of a wrinkled gold surface. One of the reasons for using this material as a conductive electrode is its low resistance. Also, because of its softness or low elastic modulus, gold can be shaped in several forms without cracking. The other reason for using this material is its ease to be coated with a Sputtering machine. Sputtering is an appropriate technique to make gold substrate in any thickness.

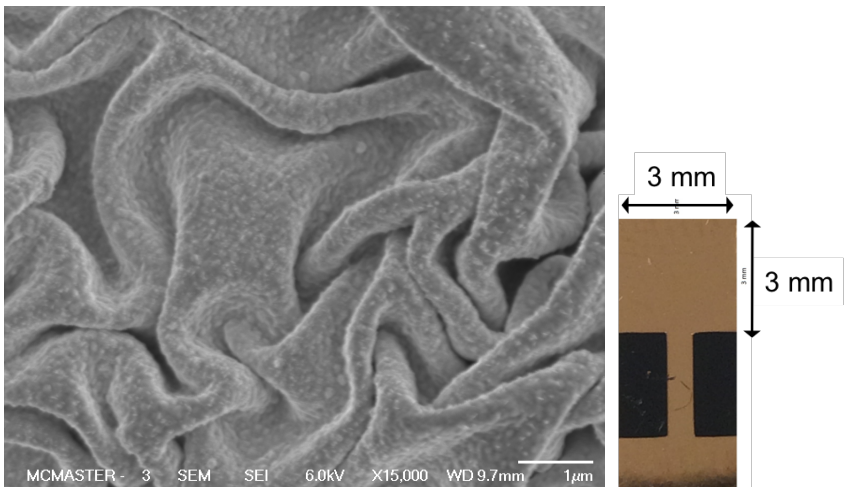

Figure 3.1: SEM (Left) and Light Microscope (Right) images of Wrinkled gold.

As it is seen from Fig. 3.1, wrinkled gold is a good material to be used as the working electrode due to the high surface area. The method for producing this wrinkle

gold is straightforward. Firstly, gold is sputtered (20 nm) on the polystyrene sheet. This polystyrene is pre-strained, thus, by heating, the polystyrene is shrunk to a wrinkled form and returns to its original dimensions. The dimensions of the electrode before heating are 5 mm in width, 10 mm in length and 0.1 mm in thickness. After heating in the oven (150 ° C for 3 minutes), these dimensions are reduced to 3 mm, 6.5 mm and 2 mm, respectively. The exposed surface of the electrode inside the solution is 3 mm x 3 mm as seen in Fig. 3.1. According to the shape of the electrode, the active part is joint through a thin band to the small part of the electrode (Bottom part in Fig. 3.1). That small part is held by the clamp and connected to a potentiostat. The other electrodes in this research are the thin layer of stainless steel sheet with/without carbon coated layer.

For the electrochemical reactions, as previously stated, an electrical circuit is needed. This device includes a counter electrode, a reference electrode, and a working electrode. The device used in this research is the Gamry Reference 600+ Potentiostat. As shown in Fig. 3.2, the white cable corresponds to the reference electrode and red is the counter electrode. The black cable is used for the ground connection, and green and blue wires are related to the working electrode, which is tasked to apply voltage and reading the received voltage, respectively. The orange cable is used for the fourth electrode which is not related to this research. To complete the electrical circuit, two reference and counter electrodes are also required. A platinum electrode for the counter and Ag/AgCl electrode for reference have been selected. All solutions have been made from pure powders, $Ni(NO_3)_2$ hexahydrate with 99.999 % purity from Sigma Aldrich

(203874), $NiSO_4$ hexahydrate with 99.99 % purity from Simga Aldrich (467901), KOH 99.99 % purity and ethanol 98 %, water 99.9999 %.

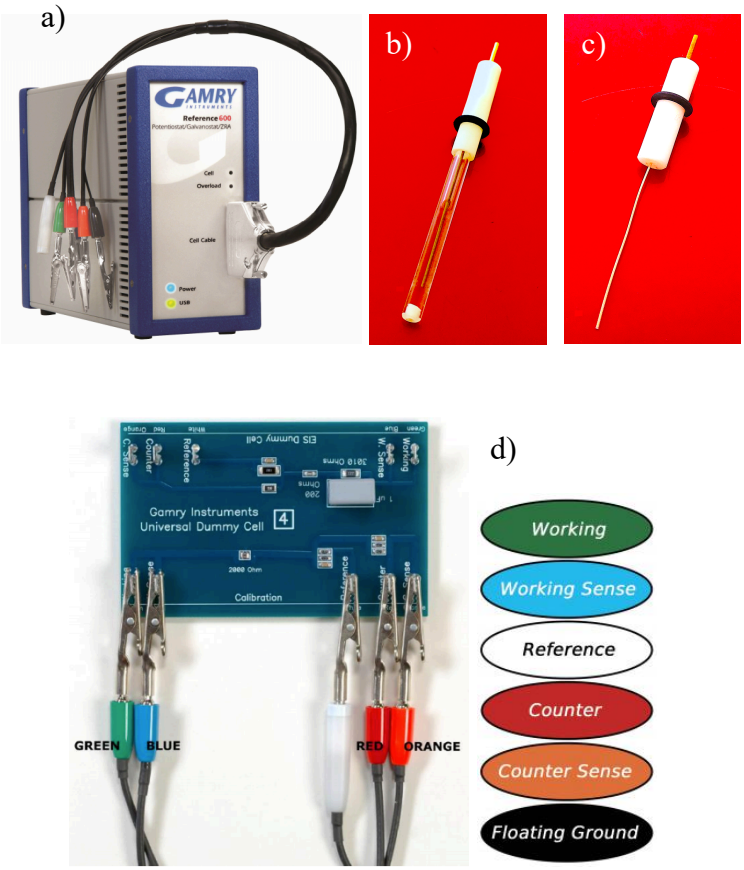

Figure 3.2: a) Gamry Potentiostat, b) Ag/AgCl reference electrode, c) Platinum counter electrode and d) the diagram with colour codes of cables in Gamry Potentiostat (Gamry Instruments, Inc., 2012).

3.2. Direct and Indirect Conditions

For the Direct method of conversion, a solution of 10 mM of $Ni(NO_3)_2$ is considered for this reaction, and the applied voltage can range from -1 volts to -2.5 volts. The chronoamperometry is done within 30 to 120 seconds. In this research, the cyclic voltammetry for the reduction and oxidation reactions for nickel hydroxide

should be done according to the following conditions. The solution is 0.1 molar KOH, and the voltage is between 0.1 to 0.6 (v). The scanning rate is 25 V/sec, and the number of cycles can range from 10 to 30 cycles depending on the time of the chronoamperometry tests.

For the Indirect method of conversion, the solution of 10 mM of nickel sulfate is used, and the voltage can be changed, as in the direct method from -1 to -2.5 volts. A dilute solution of 0.1 M KOH is used the same as the direct method. The voltage range is from 0.1 to 0.6 volts in 10 to 30 cycles.

3.3. Different Shapes of Nanoparticles and Nanowires

Using these two methods, electrochemical experiments are carried out. In the first method, known the Direct approach, the aim is to synthesize nickel hydroxide, and its characterization methods are used to observe the nanostructure, porosity and also the amount of active surface area. In the second method, referred here as Indirect approach, the conversion of nickel metal to nickel hydroxide is essential. Finally, the nanostructure and amount of modified volume, which is nickel hydroxide, is investigated. To further explore the Redox reactions, we use some other samples provided by our collaborators. Samples received from the University of Ottawa have three different nickel types namely Triangular Nickel, Urchin-like Nickel without PVP (Polyvinylpyrrolidone), and Urchin-like Nickel with PVP. The conversion process (the second step of the Indirect Method) is done for all samples. One more sample called Nickel Nanowire (90-100% from Sigma Aldrich 745561) was added to be analyzed.

Finally, the characterization tests will be carried out for all four samples. Fig. 3.3 is an overview of the samples.

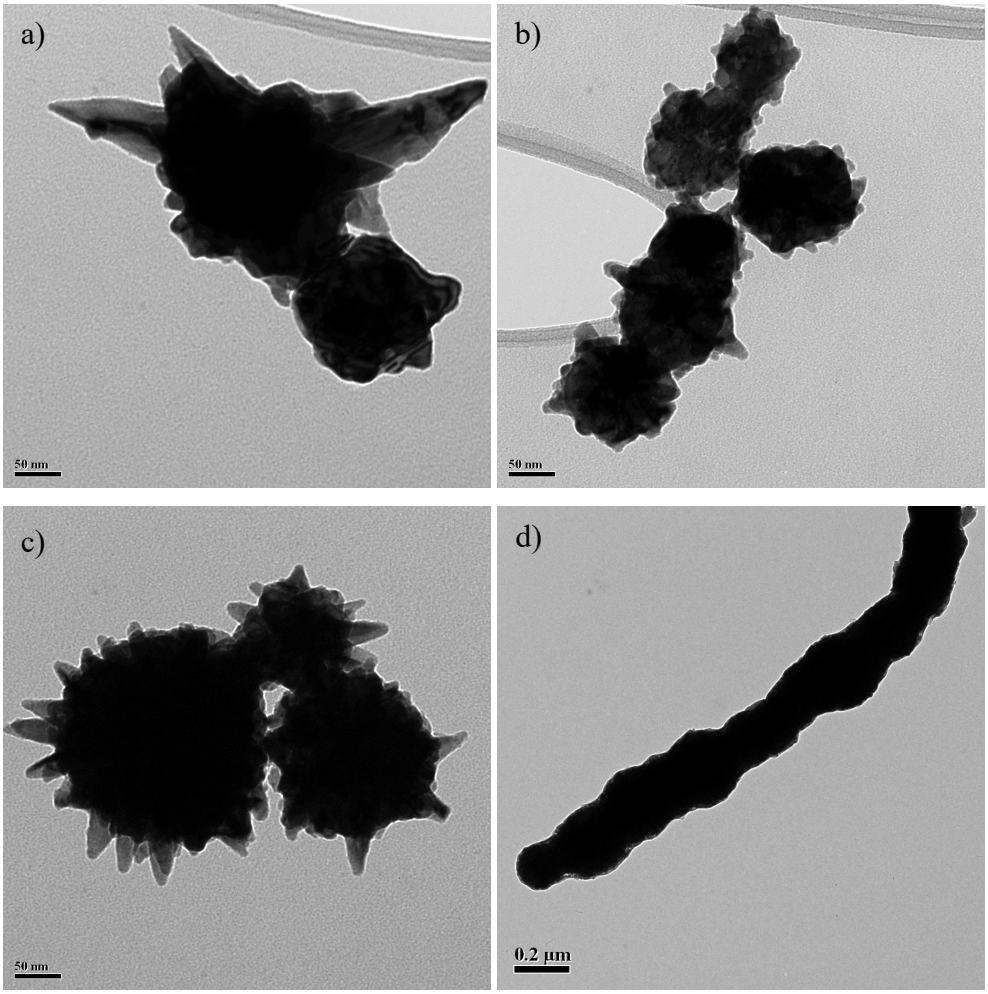

Figure 3.3: Low magnification TEM images of a) Triangular Nickel, b) Urchin-like Nickel without PVP, c) Urchin-like Nickel with PVP and d) Nickel Nanowire.

Nanoscale particles of Nickel metal are fundamental because of the high intrinsic surface area during synthesis. For instance, the needle-shaped spikes in Triangular Nickel or Urchin-like Ni with PVP prevent each other from strongly packing with each other due

to the very irregular shape and ligands preventing strong packing of smaller particles. Therefore, due the space between particles, it is expected that the electrolyte can easily penetrate through structures and increase the reaction efficiency as shown in the results section.

3.4. Sample Preparation for Electron Microscopy Analyses

Once the specimens have been synthesized, it is necessary to prepare the samples for electron microscopy tests. In this step, several techniques are proposed and, depending on the type of analysis, the sample preparation is different.

For SEM analyses, the electrode must be conductive. As stated in section 1.1, the gold electrode is located on a layer of polystyrene. This polymer is non-conductive, so either a carbon coating or nickel paste should be used to make this sample conduct incident electrons to the ground for optimal imaging. A nickel paste is much more convenient and more accessible in the laboratory, and also has more conductivity; thus, it prevents the sample from being charged and any damage due to the electron beam. The nickel paste is positioned in full contact with the active part of the electrode and then on a stub. Therefore, electrons can go through this path to ground.

For TEM tests, nanoparticles are required to be placed on a copper grid. The first step is to scratch the deposited particles from the surface of the working electrode using a blade. Then, the particles can be moved to a container using few droplets of pure ethanol. Usually, the container of solutions should be sonicated between 10 to 15 min to prevent agglomeration. Then a droplet of solution is dropped on holey carbon

copper grid and then dried out using gentle heating from an incandescent light. These particles are dispersed on the grid. The solution used here is ethanol because it is easy to be dried on the grid, and is it a not a good solvent of nickel hydroxide (Ni-based nanoparticles must not be dissolved in ethanol).

3.5. Electron Microscopes Specifications

The JEOL JSM-7000F with Oxford 50 mm^2 EDS detector is used for SEM analyses. This instrument is equipped with Schottky field emission gun which operates at 1 KV to 30 KV. For HRSEM analysis, the FEI Magellan 400 is used. The resolution is better than 1 nanometer.

The JEOL 2010F TEM/STEM is one of the high-resolution microscope that is used for Electron Diffraction. This microscope operates at 200KV with FEG (Field Emission Gun). For HRTEM and Tomography, the Titan 80-300 LB is used operating at 80 – 300 KV. This is image-corrected STEM and High Resolution TEM with monochromator.

3.6. Methodology of Tomography

Tomography is done by TEM with monochromator in Dark Field to get more contrast in STEM mode. Particles should be settled down on Holey copper grid. Specific Holder is needed that allows us tilt the sample from -64 to +64 degrees. All data should be stored on one file to reconstruct them with Inspect 3D that is released from FEI company or TomoJ plugin which can be installed to ImageJ. After

reconstruction in SIRT format that produces slices of sample, these slices are ready to create 3D model with visualization applications such as TomViz or Amira. To review the procedures of tomography, one of the samples from this thesis is used. The procedure is as follows:

After sample preparation for TEM, then you can load the holder and insert it into microscope. After alignment of the microscope in STEM dark-field mode, images are captured automatically with tilt angle from -64 to +64 (Auto-focus is done for each image). An example is seen in Fig. 3.4.

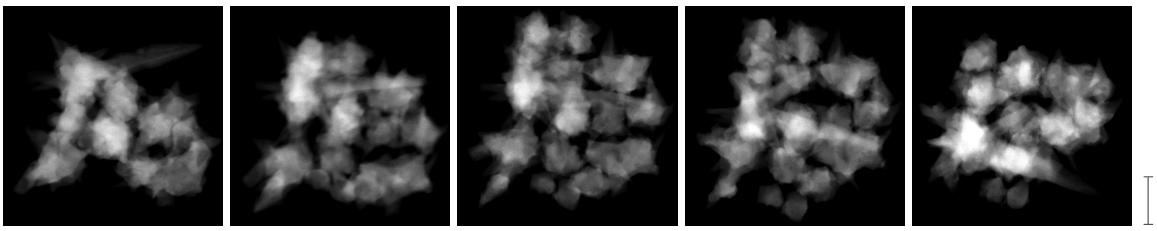

Figure 3.4: TEM tilted images from a Tomography dataset extracted at -54, -22, 0, 22 and 54 degrees from left to right, respectively. The scale bar on the right of the set of images is 200 nm.

All images are saved in one file but they need to be aligned with respect to each other for optimal reconstruction. All images must be stacked in one axis of tilting by generating landmarks. Landmark chains are markers in images which track the images' movement to stack them all in single tilt axis (Sorzano *et al.,*2009). Variables in landmarks and alignments are strongly dependent on shape, size and resolution. Consequently, reconstruction can be started when all images are realigned with respect to one single axis to create tomogram that is used for modelling. One common reconstruction algorithm is SIRT which is based on number of iterations that have been

computed to resemble projections when images were formed in microscope. According to the literature, at least 4 iterations are needed to make a proper tomogram; however, more iterations does not mean better efficiency (Messaoudi *et al.,* 2007). Therefore, up to 30 iterations are not recommended. For instance, Fig. 3.5 shows selected slices from a reconstructed tomogram volume containing 836 slices.

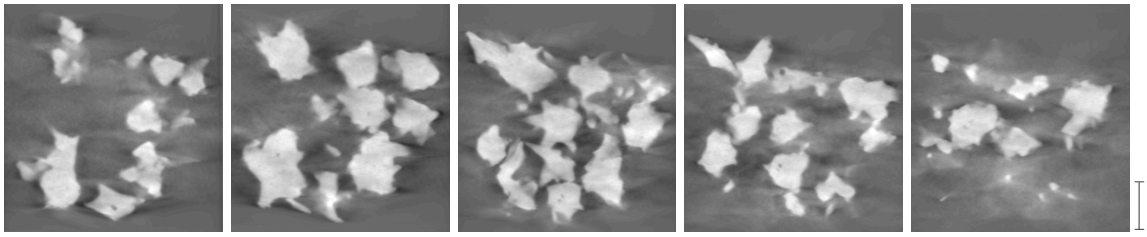

Figure 3.5: Slice number 300, 350, 400, 450 and 500, respectively from left to right.The scale bar is 200 nm.

The generated file is in .SIRT format and compatible to run in any visualization software. TomViz is a free software for this purpose. By opening the file and making a contour of block, a 3D model is formed (Fig. 3.6). A scale bar can be added in 3D space; some procedures can be carried out after the reconstruction such as filtering, adjusting thresholds, analyzing volumes, surface areas etc.

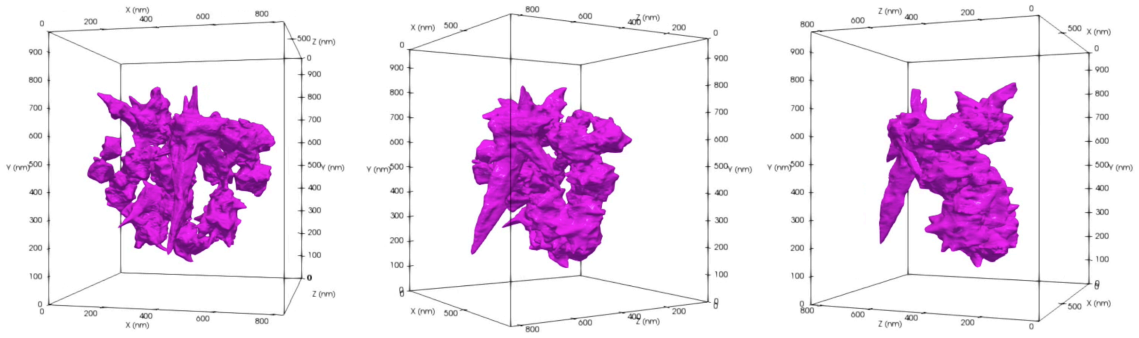

Figure 3.6: 3D model of particles in 10, 60 and 100 degrees, respectively from left to right.

4. Results and Discussions

In this section, we have prepared 6 samples as follows:

- Sample No. 1: The first specimen was prepared with the Direct approach on wrinkled gold substrate (Discussed in chapter 3). The deposition time for this sample was 120 seconds, and the applied voltage was -1.6 V. The conditions for the cyclic voltammetry were 20 cycles, a voltage range of 0.1 to 0.55 volts, and a scan rate of 25 mV/s.
- Sample No. 2: The second sample was prepared in Indirect approach on wrinkled gold substrate. The deposition time was 120 seconds, and at a voltage of -1.4 V. The number of applied CV cycles is 20, the voltage range is from 0.1 to 0.5 volts, with a scan rate of 25 mV/s.
- Sample No. 3 and 4: These two samples have been prepared in the same conditions as samples No. 1 and 2, respectively. The only difference is stainless steel substrate which was used.
- Sample No. 5 and 6: These two samples were prepared in the same conditions as sample No. 3 and 4, respectively. The only difference is number of CV cycles, which was 15 cycles.

4.1. Characterization via SEM and EDS Analyses

According to Fig. 4.1 for sample No. 1, the film is not fully dense and the nanoparticles are not completely spherical, but their porosity between the particles

would increase the active surface area and provide greater surface for reactions with the electrolyte. Even though the nanoparticles are not entirely spherical, their diameter can be approximated to be, on average, 180 nm. As seen in the EDS analysis (Fig. 4.1), there is a significant amount of nickel as well as oxygen on the deposited layer.

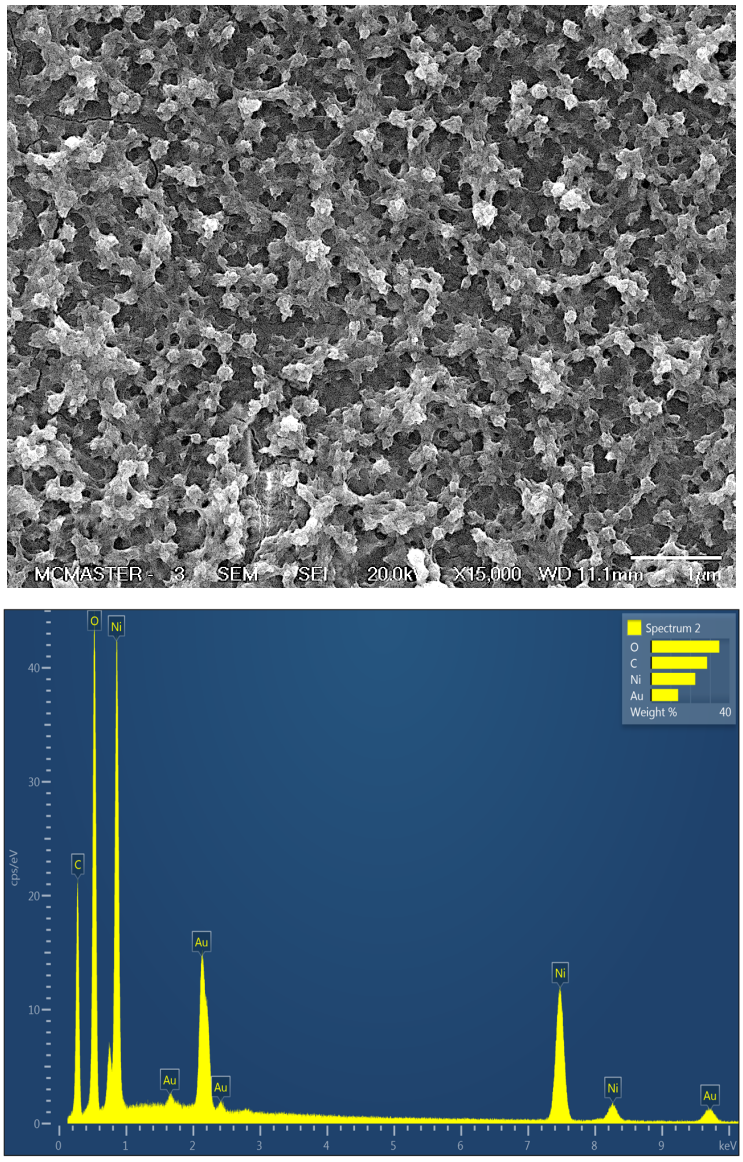

Figure 4.1: SEM Image of α-Ni(OH)$_2$ (Top), EDS spectrum (Bottom).

Fig. 4.2 shows that the maximum current for the oxidation reaction is initially decreasing (first curve: blue), but after the third cycle (purple curve), it increases. This means that with increase in the number of CV cycles, the amount of nickel hydroxide involved in the reaction is increasing. In other words, at each cycling time, the electrolyte adjacent to nickel hydroxide is more likely to react. This interesting point was the subject of further experiments.

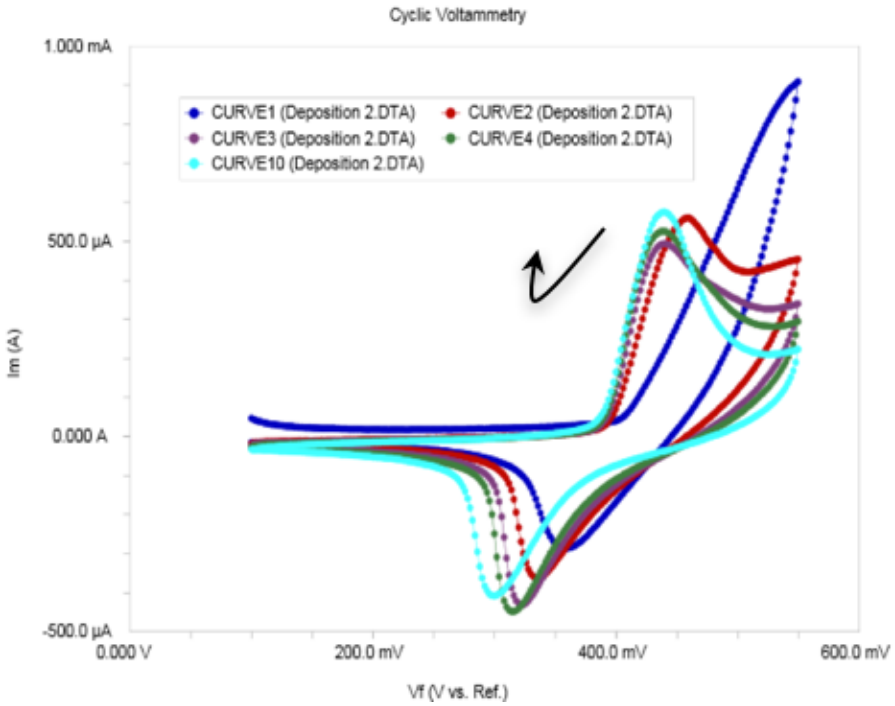

Figure 4.2: CV curve of Direct method including cycles number 1 to 4 (Blue, red, purple, green, respectively) and 10 (Turquoise).

Meanwhile, sample No. 2, which is prepared in Indirect approach, is examined. As shown in Fig. 4.3 (Top), nickel metal particles are deposited on the surface. The average diameter of these particles is 157 nm. Then, by performing cyclic

voltammetry, the final structure of the nickel hydroxide appears to be formed as grape-shaped nanocrystals (Fig. 4.3 Bottom).

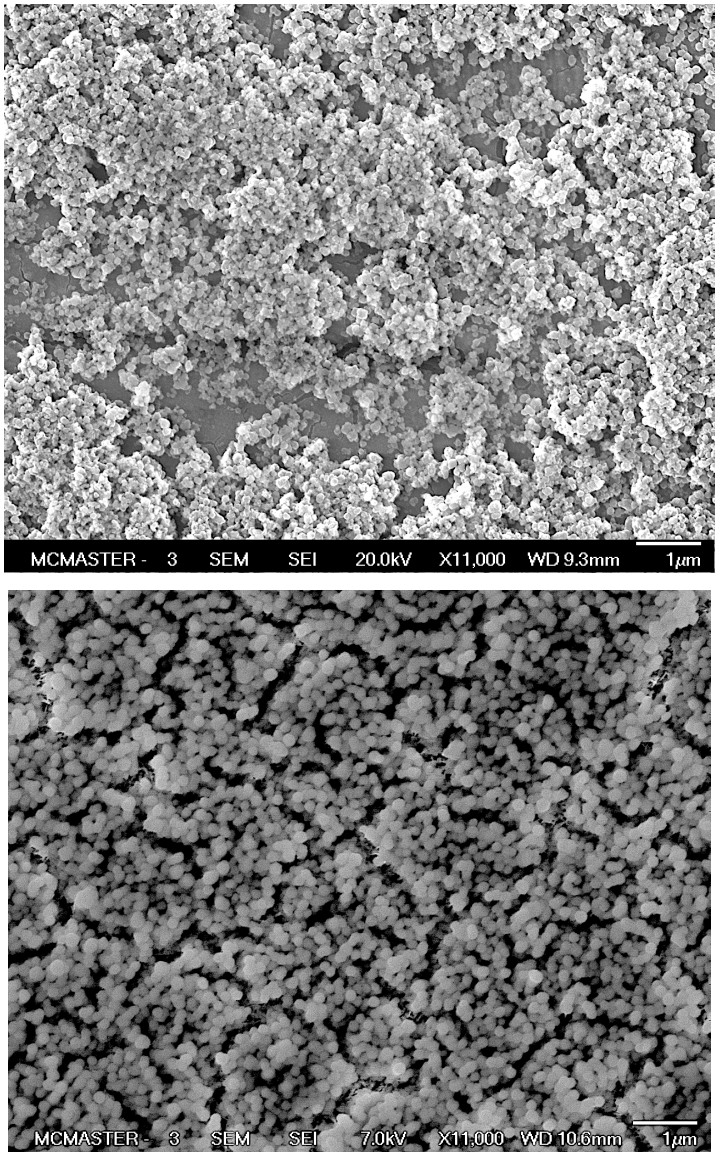

Figure 4.3: SEM Images of Indirect method before (Top) and after (Bottom) conversion.

The EDS analysis in Fig. 4.4 also shows the fraction of nickel (Top) and nickel hydroxide (Bottom) in the structure. We note that we detect the Au peak from the

wrinkled Au substrate, indicating the penetration of the electron through the deposited film. The intensity of the peak for nickel metal before conversion was more significant (Top EDS spectrum in Fig. 4.4) than after conversion, but after CV experiments, a significantly stronger oxygen peak can be detected (Bottom) and a weaker Au signal is also detected. In this case, the average particle diameter is ~170 nm. In this structure, in addition to the size of the nanoparticles, the dispersion and porosity are very important. When nickel is deposited on the surface, for the cyclic voltammetry, the electrolyte can easily penetrate through the structure and increase the Redox reactions.

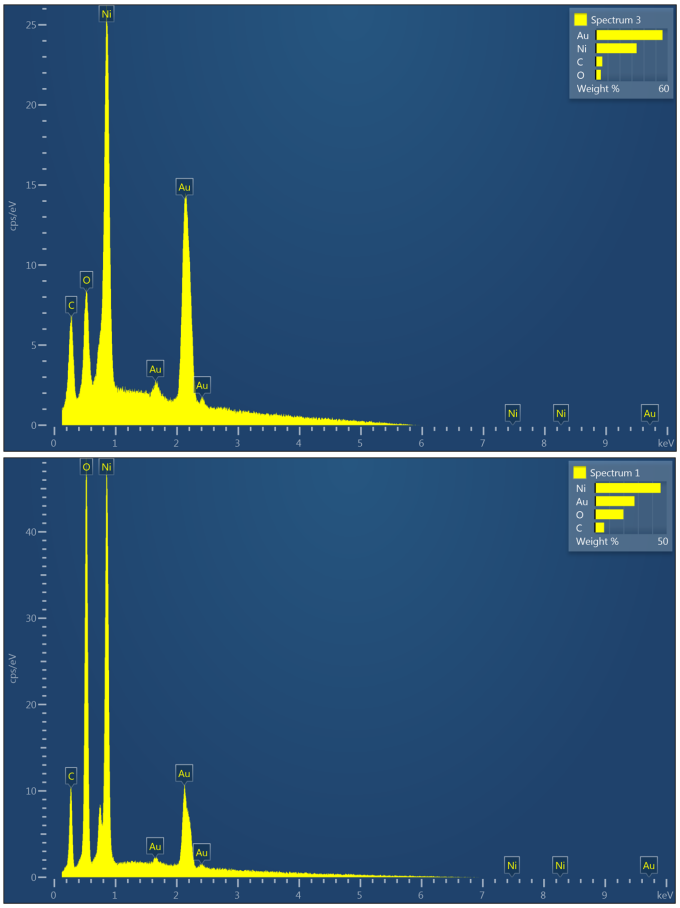

Figure 4.4: EDS spectra of Indirect method before (Top) and after (Bottom) CV.

In the cyclic voltammetry curve (Fig. 4.5) for this sample produced with the indirect approach, similarly to the Direct method, the oxidation current first decreases and then increases, which is expected.

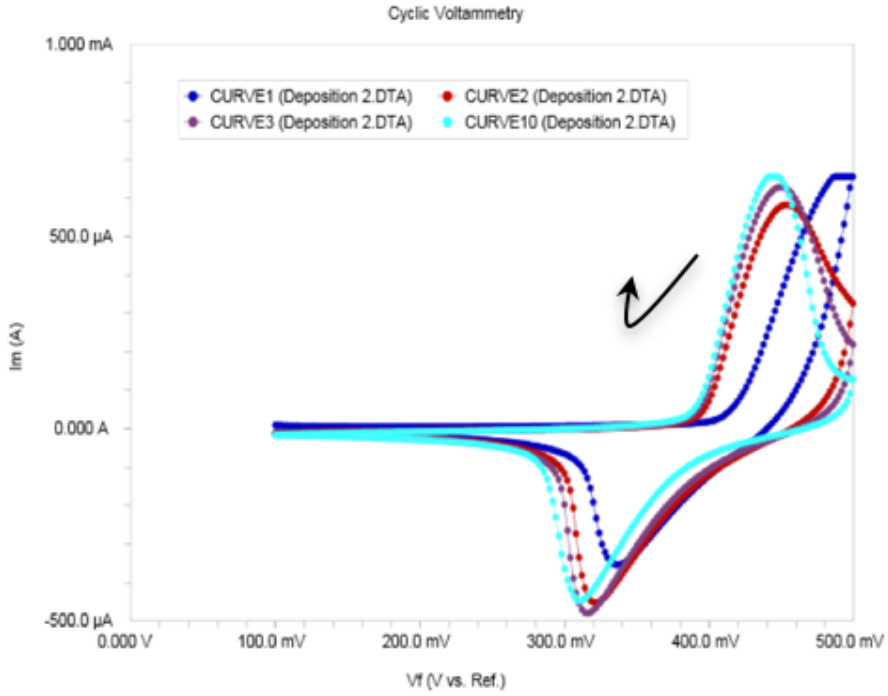

Figure 4.5: CV curve of Indirect method including cycles number 1 to 3 (Blue, red, purple, respectively) and 10 (Turquoise). First cycle can be done to remove any passive layer or contaminations.

As described in Eq. 2.9 and 2.10, nickel is converted to nickel hydroxide in the reaction, but this reaction is irreversible. Thus, at each cycle, a new volume of nickel hydroxide is produced and then reacts in response to the electrolyte and electrochemical reaction. By increasing the thickness of hydroxide, the diffusion rate of hydrogen and oxygen through hydroxide layer will control the kinetics of the reactions and the speed of reactions decreases. So, Redox reactions need adequate

time, or higher CV cycles or lower scan rate of CV to be done. At the end, the conversion process is continued to convert all amount of nickel to $Ni(OH)_2$ in higher. The drop in current in the first and second cycles could be due to polishing of an oxide layer or removing passive layer.

For this sample, there are several questions that should be investigated: firstly, why is the amount of nickel hydroxide that is participating in the reaction increasing during CV in the Direct method. Secondly, why is the size of nanoparticles increasing after CV following synthesis with the Indirect method. To address these questions, CV was used. For this, we initially prepared two samples in the same way (the first stage of the deposition, or Chronoamperometry), and then we put half of the electrodes into the solution for cyclic voltammetry. With this approach, a portion of the electrode in the cyclic reaction does not react and the effect on the nanostructure is also shown on exactly the same starting material.

4.2. Different Structure with and without CV

New samples (No. 3 and 4) with different substrate (Stainless steel) have been prepared. Fig. 4.6 is related to sample No. 3 in Direct method and the image is taken at low magnification (Left) and high magnification (Right) from the boundary. The sample exhibits significant differences before and after CV. The nickel hydroxide as deposited does not have any particle structure (it appears as a continuous film) and is present as a layer on the surface prior to CV. However, once it is reacted following CV

in the electrolyte, this layer begins to crack, and the nanoparticles begin to grow in the form of a quasi-sphere.

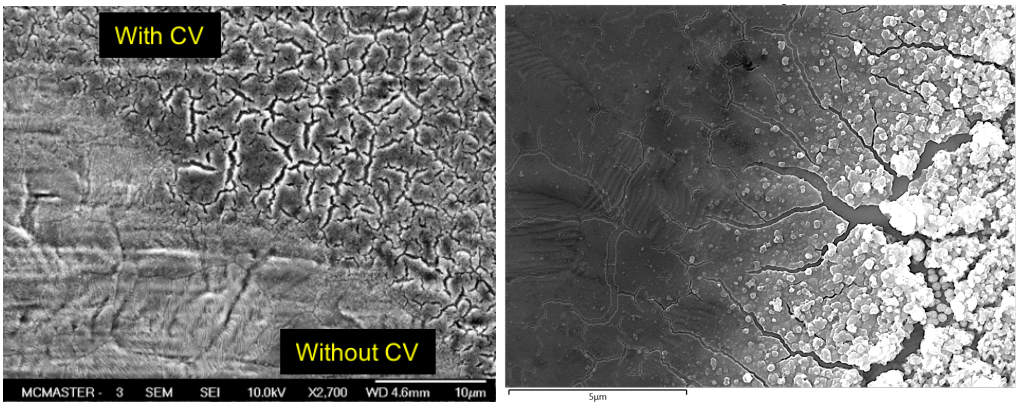

Figure 4.6: Sample No. 3 prepared by Direct method with 2 different regions, with or without CV.

An explanation for the changes in the CV experiments can therefore be given. During the first cycles, the current decreases which is due to removing contaminations and polishing oxide layer. Then, nickel hydroxide is in the form of a layer and the electrolyte only contacts the outer surface, so the surface area of active material is very low. However, by creating cracks and forming spherical clusters in the form of nanoparticles, the level of contact increases. So, the reason for the increasing peak in the series of CV experiments is due to this change in the nanostructure. This is the first general conclusion that the alpha-phase structure can initially be a continuous structure with low porosity, but during the CV, this structure can be changed. By increasing the number of cycles in CV, the structural changes increase.

This evolution does not apply for the Indirect method. As shown in Fig. 4.7 for sample No. 4, there is no structural difference before and after CV. With HRSEM

analysis in following, this would be more clear. The structure in both cases is spherical nanoparticles, with their only difference being the particle's diameter and the brightness of the images. The nickel hydroxide is brighter due to more ejected secondary electrons, which are generated by the primary electron beam. Due to the presence of hydrogen and oxygen elements, the small particle size (more secondary electrons can escape from a small particle), there is an overall increase in secondary electrons yield. Also, charging of the sample might increase the brightness.

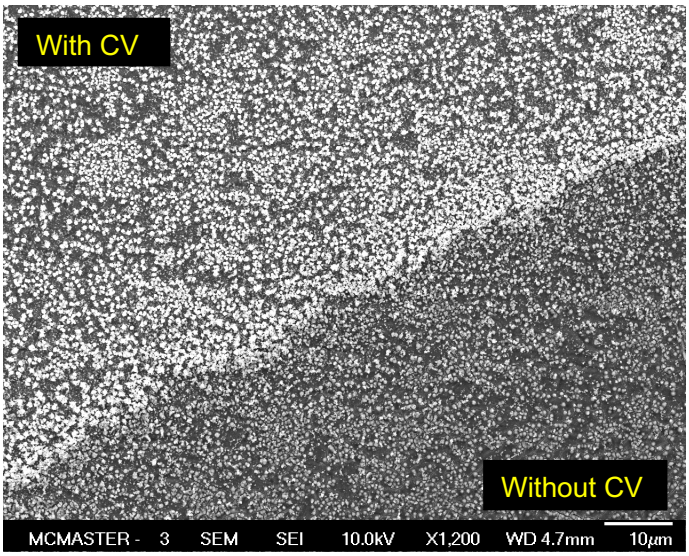

Figure 4.7: Sample No. 4 by Indirect method with 2 different regions, with or without CV.

4.3. High-resolution SEM Analysis

Higher magnification was also used to better visualize the nanoparticles using the high-resolution SEM (HRSEM). For this work, new samples (No. 5 and 6) were developed using a similar approach to the previous set of samples but with a different number of reaction cycles.

As shown in Fig. 4.8, imaging shows that a cyclic voltammetry reaction can change the morphology of the deposited layer from a continuous coating without any porosity to pseudo-spherical structures. One of the reasons might be generation of micro-bubbles. In this case, the average diameter of the nanoparticles is 88 nm.

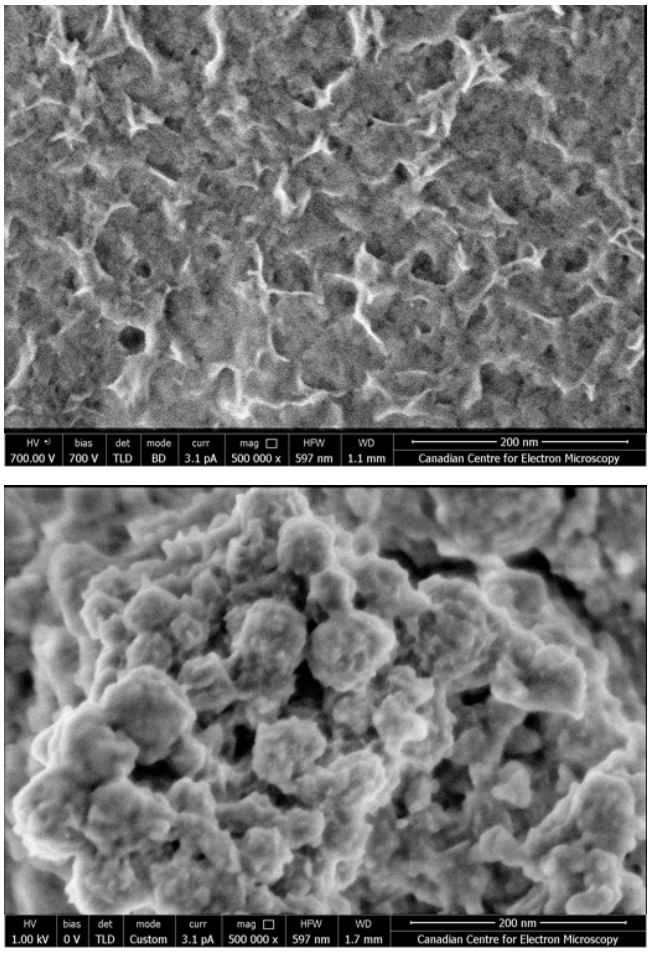

Figure 4.8: Sample No. 5 prepared by Direct method before (Top) and after (Bottom) CV.

In sample No. 6, as previously stated, the structure is similar before and after conversion, which is spherical with porosity (Fig. 4.9). The only difference is the expansion of these particles. The formed layer on the surface is nickel hydroxide which

has a larger lattice parameter. This causes an expansion due to the formation of the hydroxide layer. By doing 15 CV cycles, the diameter of particles becomes ~ 90 nm.

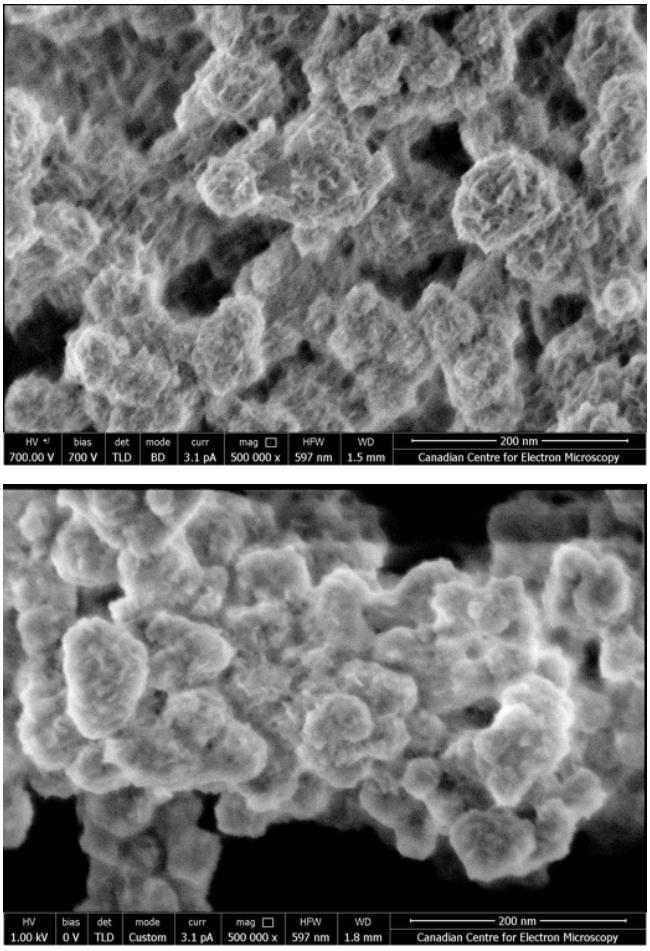

Figure 4.9: Sample No. 6 prepared by Indirect method before (Top) and after (Bottom) conversion or CV.

For these materials the biggest challenge is related to the elemental analyses since hydrogen is undetectable although nickel and oxygen are present in both phases. Therefore based on the oxygen content (even if the measurement were precise enough), it would not be possible to identify whether $Ni(OH)_2$ or NiO_2 is present just from the chemical analysis alone without any assumptions on the existence of these phases. Due

to the high speed of the oxidation reaction (the synthesis of samples is carried out with large supply of the electrolyte on a porous material), we expect that the presence of nickel oxide presence is likely. However, it is also possible that the oxide is reduced during the CV with KOH. Therefore, given these arguments, it is necessary to ascertain the presence of the hydroxide phase $Ni(OH)_2$ by alternate methods as shown in the next section.

4.4. Electron Diffraction Analysis

The reference diffraction pattern of both nickel hydroxide phases (alpha and beta) can be extracted from the database. We used the JEMS software to analyze the patterns. It is easy to prove that the structure is not nickel oxide. Samples No. 5 (Direct) and 6 (Indirect) were chosen for diffraction tests before and after the CV experiments. Fig. 4.10 which corresponds to sample 5 before CV, the structure is a layer (i.e. plate like) and not spherical shape.

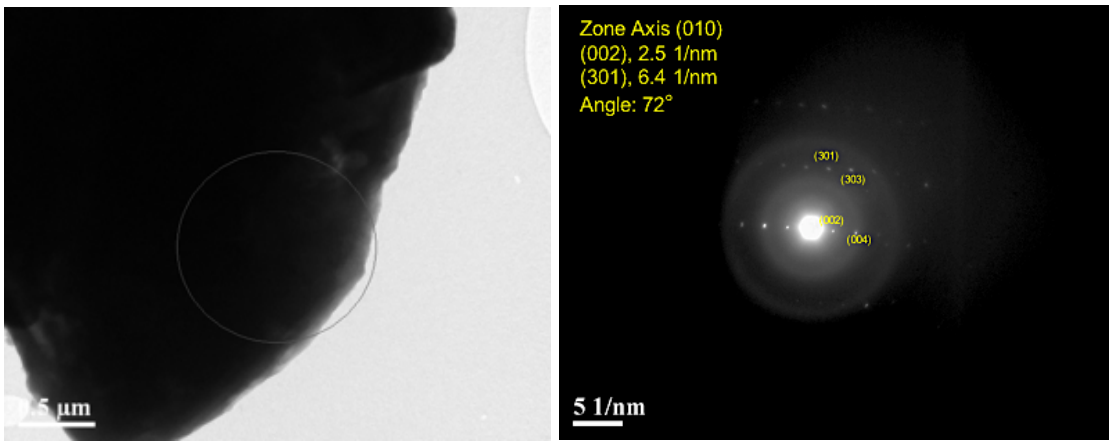

Figure 4.10: Diffraction pattern of sample No. 5 from single crystal of α-$Ni(OH)_2$.

Its diffraction pattern consists of a spot pattern overlapping with diffuse rings originating from background support which is carbon. The single crystal pattern can be indexed to be originating from the (010) zone axis. The major reflections are indexed as shown in the overlapping indexes within the JEMS software.

However, the same material, after CV cycling is polycrystalline as shown in Fig. 4.11 since the pattern consists of several spots along rings. These rings correspond to the alpha-nickel hydroxide crystalline planes.

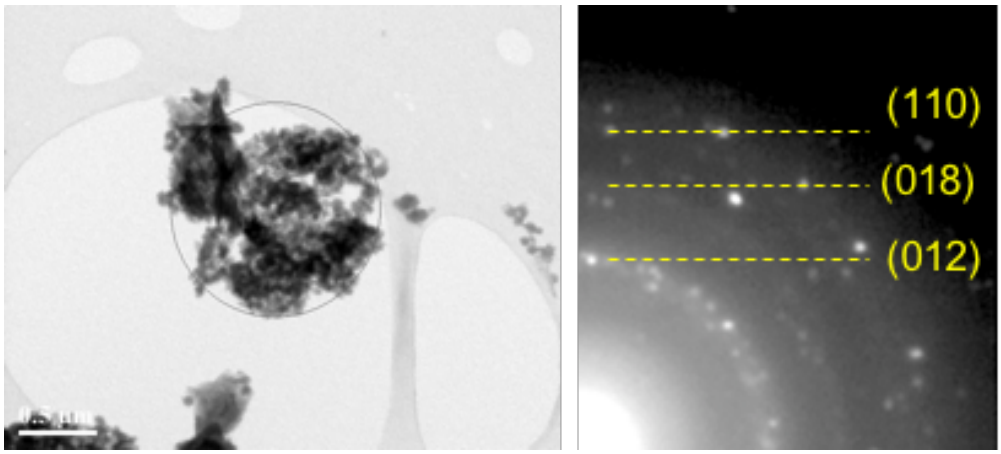

Figure 4.11: Diffraction pattern of sample No. 5 from particles of α-$Ni(OH)_2$.

Fig. 4.12 and 4.13 show sample number 6 before and after CV. As seen in both cases, there is a ring diffraction pattern due to the particle structure. Before the CV (Fig. 4.12), the pattern is the nickel entirely. However, after the CV (Fig. 4.13), there are additional rings. By overlapping the patterns, it can be concluded that the particles are composed of nickel and nickel hydroxide crystalline planes. This means that particles still contain nickel, and all nickel has not been converted.

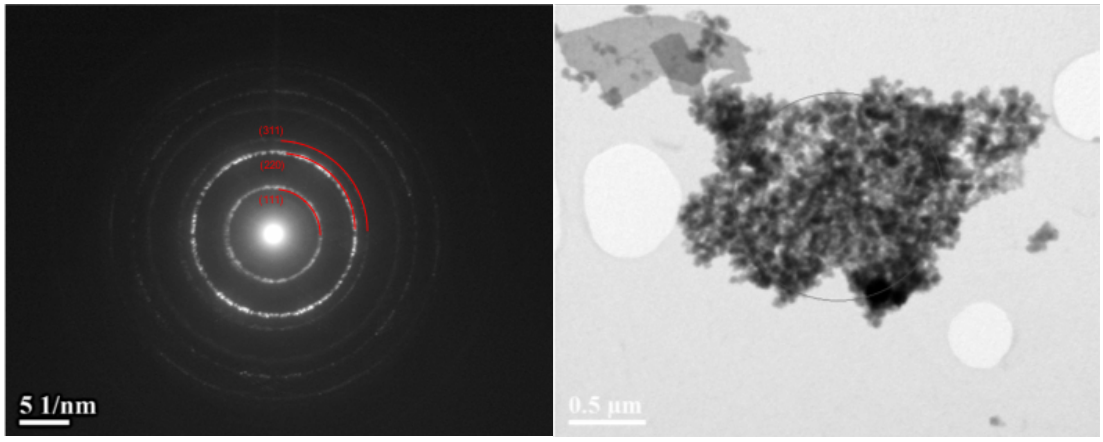

Figure 4.12: Ring pattern of sample No. 6 before conversion.

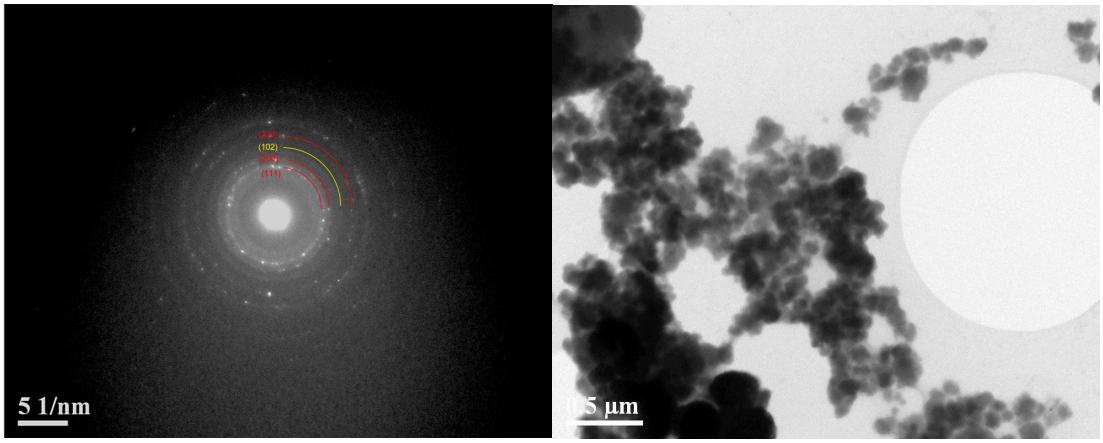

Figure 4.13: Ring pattern of sample No. 6 after CV including 2 overlapped patterns of Ni and β-$Ni(OH)_2$.

4.5. Atomic Resolution Imaging and Structure Identification of α and β Nickel Hydroxide by HRTEM

To visualize the co-existence of the two crystalline the structures in real space, high-resolution TEM (HRTEM) is needed. The procedure consists in capturing an image with the high-resolution mode of the microscope. Since the crystal planes can be identified from the Fourier Transform (FT), the equivalent of a digital diffraction

pattern (or diffractogram), the phases can be identified. After selection of specific reflections corresponding to the phase of interest are selected, the inverse FT (IFT) can be used to reconstruct the equivalent of a dark-field image of the phase that was selected from the diffractogram. All this can be done within Digital Micrograph, a software for microscopy developed by Gatan, the nickel and nickel hydroxide planes are identified and mapped using the IFT image. Lastly, by using information from the database, those planes can be indexed or shown together using RGB contrast with each phase using a colour (for example, green for alpha phase, red for Ni). Fig. 4.14 shows the HRTEM image of sample No. 5 in Direct method. The surface contains very fine crystals, which are identified as the alpha-nickel hydroxide phase. Planes (111), (200) and (110) are also visible in the image with specific $D_{spacing}$ that were confirmed with the use of the database. It can also be shown by using RGB (Fig. 4.15) that the whole structure is relatively single-phase alpha-nickel hydroxide but polycrystalline.

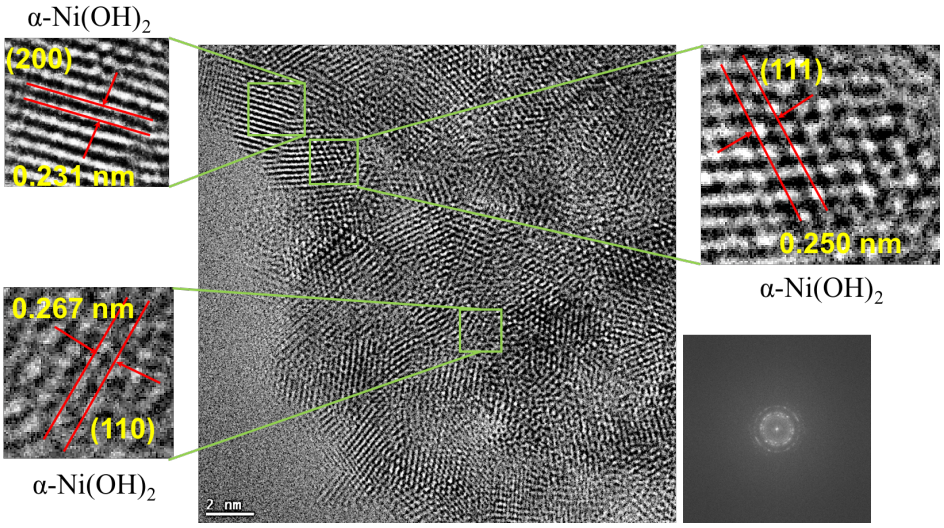

Figure 4.14: HRTEM image of α-Ni(OH)2 and FFT.

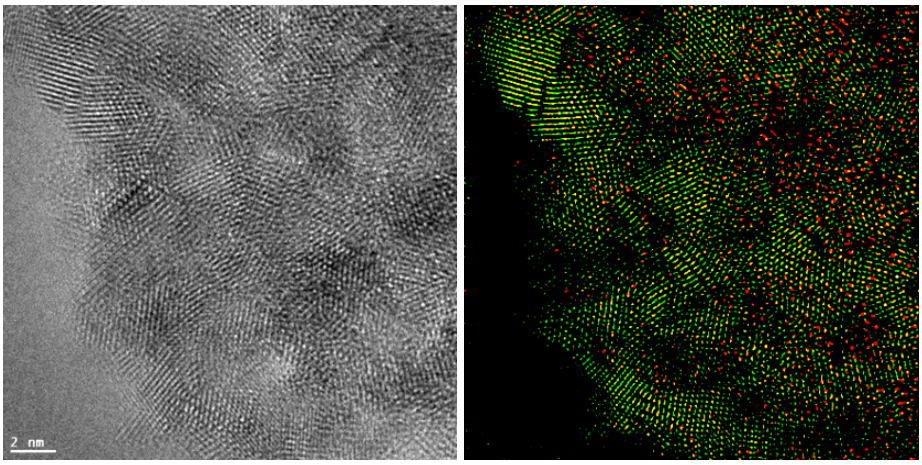

Figure 4.15: HRTEM and RGB Contrast images. Green (α-$Ni(OH)_2$), Red (Amorphous phase).

In sample No. 6, as described in the previous section, both nickel and nickel hydroxide structures are present (Fig. 4.16). The crystalline structure of beta-nickel hydroxide, which is hexagonal, is entirely different from nickel that is FCC.

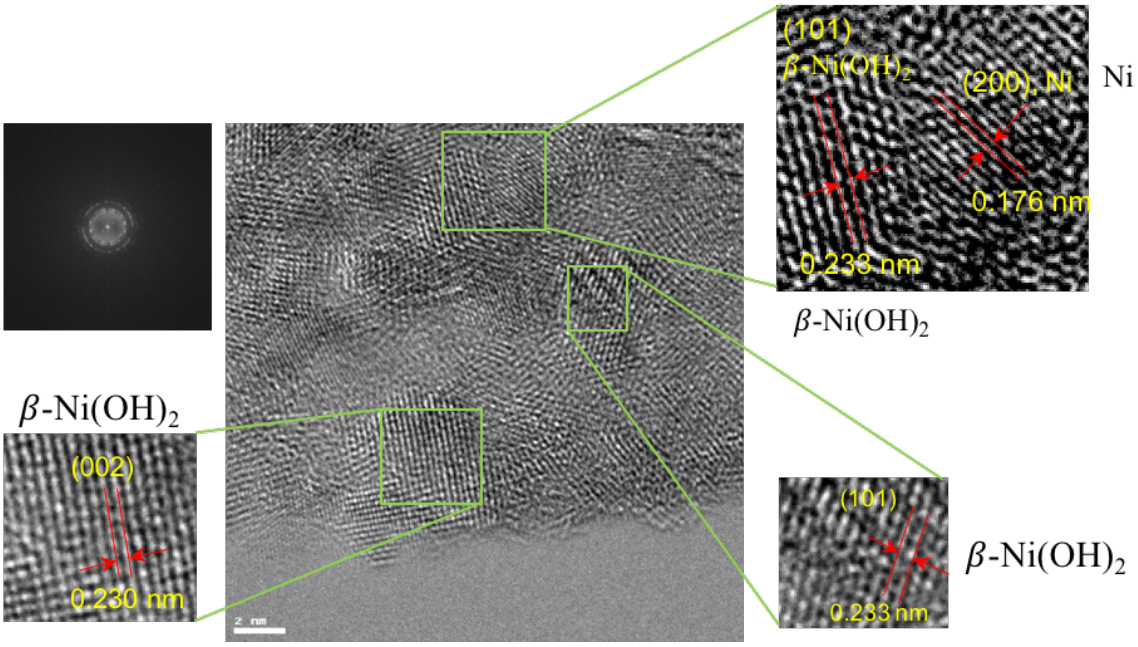

Figure 4.16: HRTEM image of β-$Ni(OH)_2$ and Ni and FFT.

The difference between the two phases is visible only in few reflections. In the image, nickel hydroxide planes are indexed and wholly separated from nickel planes. As seen in the RGB image (Fig. 4.17), both nickel and beta-nickel hydroxide co-exist.

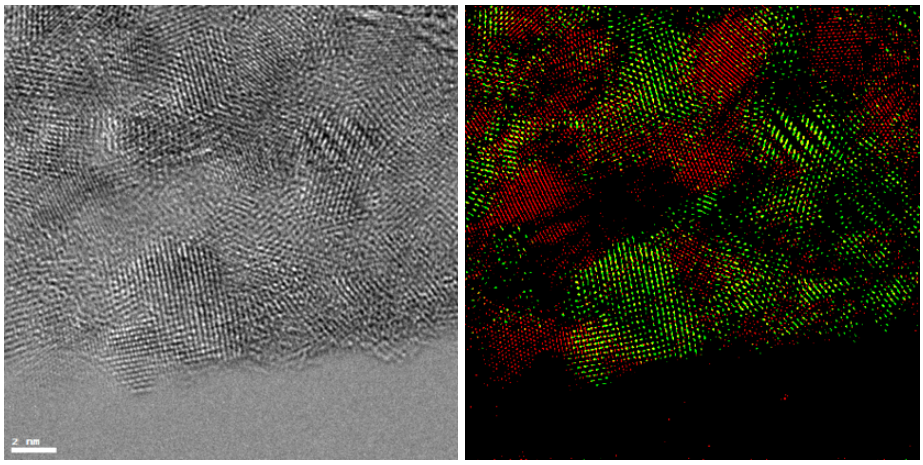

Figure 4.17: HRTEM and RGB Contrast images. Green (β-$Ni(OH)_2$), Red (Nickel).

4.6. Different Shape of Nickel Nanoparticles

In this section, we investigate different phases prepared by our collaborators at the University of Ottawa to understand the different morphologies of beta phase. As explained earlier, the most stable phase for the alkaline reactions in Ni is the beta phase. So far, the synthesis of this phase has been carried out, and the necessary conclusions have been made. In our work we investigate the conversion of nickel to nickel hydroxide with these different samples with names identified by our collaborators as: “Triangular” and “Urchins”. These are used for glycerol electro-oxidation to transform wastes into value added chemicals. Also it could be used in batteries and fuel cells in addition to electrocatalyst. Here is the summary of

procedures of these materials. Nickel nanoparticles are synthesized by hydrazine reduction. For triangular nickel, Nickel (II) chloride hexahydrate is dissolved in ethylene glycol (50 mM). Then, 0.1 M of hydrazine (50-60 % purity) is added. By adding hydrazine, Ni-hydrazine complexes $[Ni(N_2H_4)_2]^{2+}$ is formed. According to Eq. 4.1, Ni nanoparticles are formed by injection of 1.5 ml of 0.1 M NaOH into the solution.

$$2Ni^{2+} + N_2H_4 + 4OH^- \rightarrow 2Ni + N_2 + 4H_2O \qquad \text{(Eq. 4.1)}$$

Then, the solution is kept at 100^o C for 30 min and cooled to room temperature. For urchin nickel, the procedure is similar but concentrations are different; in addition, the solution is maintained at 100^o C from the beginning. The amount of hydrazine to be added to the solution is 1.7 mM. After formation of Ni-hydrazine complexes, 4.5 ml of 0.5 NaOH is injected. This procedure is also done with different concentration of PVP which causes synthesis of urchin Ni in different shapes.

The indirect method is straightforward and can be applied to nickel prepared in different nanoscale morphologies. We therefore investigate the transformation of Ni to Ni hydroxide and how these three morphologies and change following transformation. All of these samples have been converted to nickel hydroxide in identical conditions and the equal number of cycles during CV. The voltage range of 0.1 to 0.55 volts and 20 cycles have been done. In the first step, morphological changes are examined using HRSEM before and after conversion.

4.6.1. HRSEM Images

As seen in Fig. 4.18, Triangular Nickel looks like very sharp triangular-shaped needle-like structures before the CV. After doing CV, the surface is much smoother and there appears to be a layer covering the particles, which causes an apparent expansion.

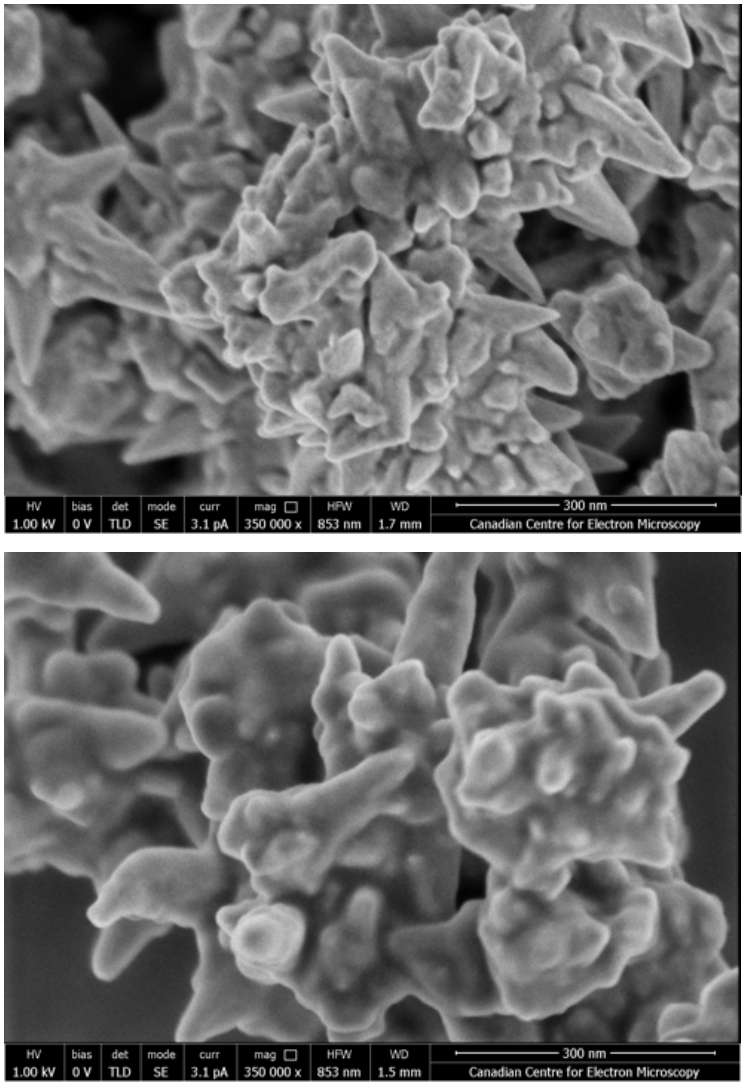

Figure 4.18: Triangular Nickel before (Top) and after (Bottom) conversion to β-$Ni(OH)_2$.

Fig. 4.19 presents the SEM micrographs of the "Urchin" Nickel particles without the PVP before doing CV. The particles appear as spheres with small extrusions, resembling an sea urchin with short spikes. After the cyclic reaction, no traces of extrusions are visible and the surface is rather rough. This nickel hydroxide layer can have a different thickness depending on the number of cycles.

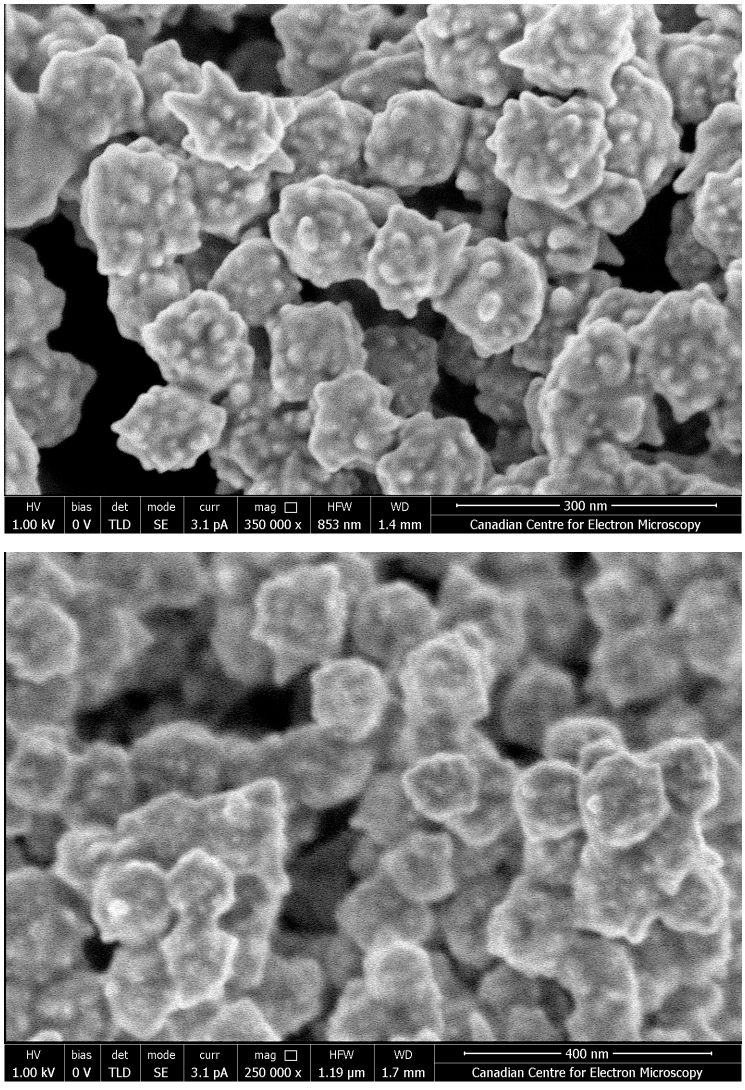

Figure 4.19: Urchin Nickel without PVP before (Top) and after (Bottom) conversion to β-$Ni(OH)_2$.

As observed in Fig. 4.20, Urchin Nickel nanoparticles, now with PVP surfactant, have sharp spikes before conversion. However, after cyclic, these spikes are no longer sharp.

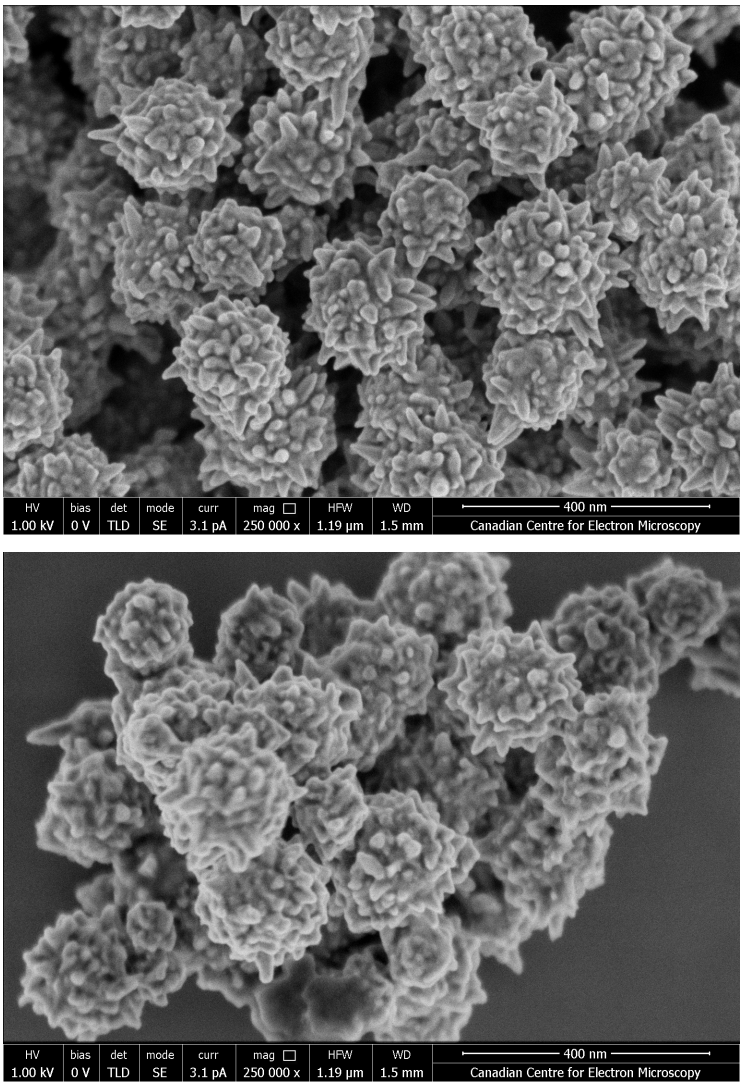

Figure 4.20: Urchin Nickel with PVP before (Top) and after (Bottom) conversion to β-$Ni(OH)_2$.

The last specimen we observed is in the form of nanowires, these were just commercially available and the diameter of the wires is 200nm before conversion.

After doing CV, the diameter becomes about 220 nm (Fig. 4.21). Thus, it is possible to approximate 10% increase in diameter by 20 cycles.

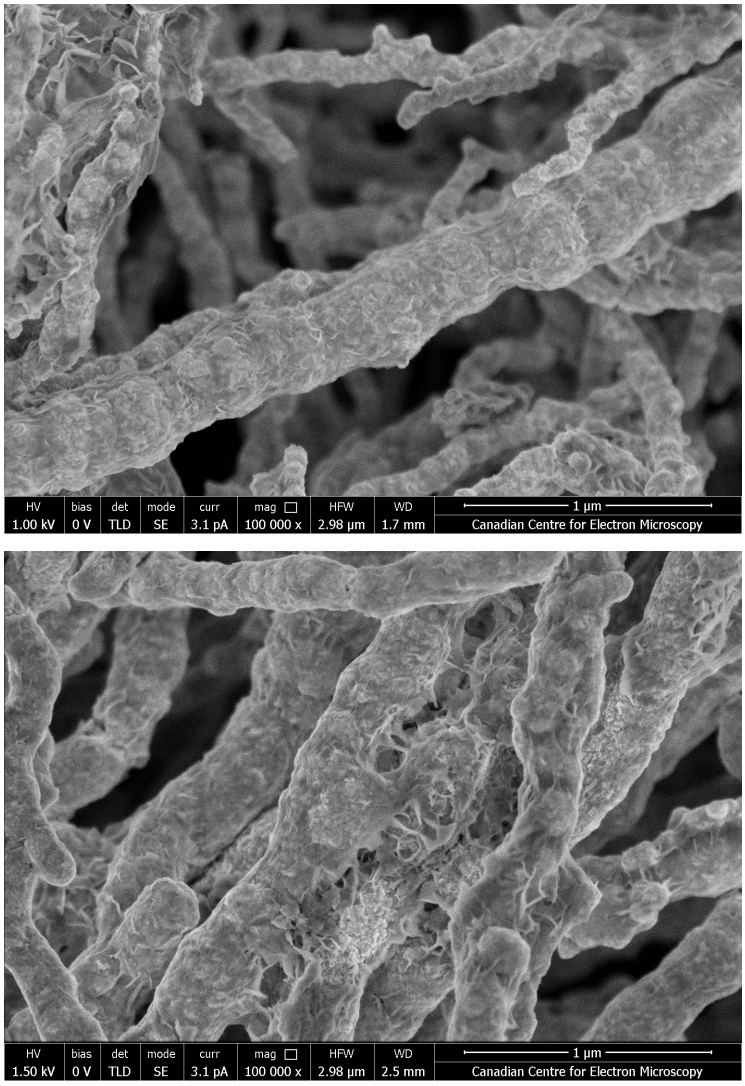

Figure 4.21: Nickel Nanowire before (Top) and after (Bottom) conversion to β-$Ni(OH)_2$.

4.6.2. Diffraction Patterns

Here, we provide evidence of the presence of nickel hydroxide using diffraction experiments. A closer look at diffraction patterns from Triangular Nickel diffraction

pattern after CV is shown in Fig. 4.22. This pattern shows evidence of reflections from nickel as well as nickel hydroxide, based on the overlay of rings on the diffraction pattern. The nickel's rings still exist in the pattern (Red rings), but the rings with yellow colour in the overlay are only consistent with the presence of a diffracting planes from beta-nickel hydroxide. While only one plane seems to be strongly visible, other planes may also exist for nickel hydroxide, but they are not detectable due to low nickel hydroxide content, as well as their proximity or overlap with nickel rings.

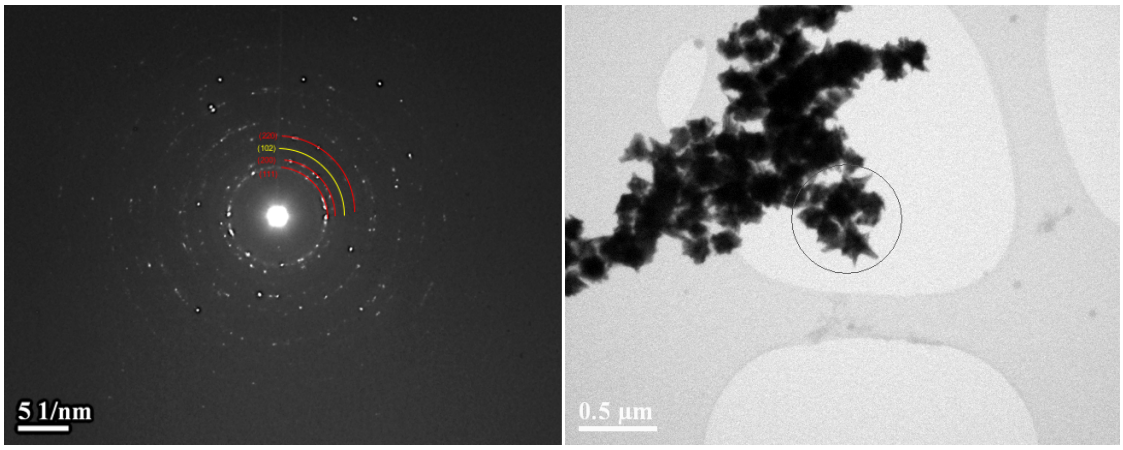

Figure 4.22: Diffraction pattern of Triangular Nickel after conversion Red reflections (Nickel), Yellow reflection (β-$Ni(OH)_2$).

Fig. 4.23 also shows the diffraction pattern of Urchin like Nickel without PVP, which is similar to the previous one, indicating the presence of residual nickel. Fig. 4.24 and 4.25 exhibit the diffraction patterns of Urchin Nickel with PVP and Nickel nanowire, respectively.

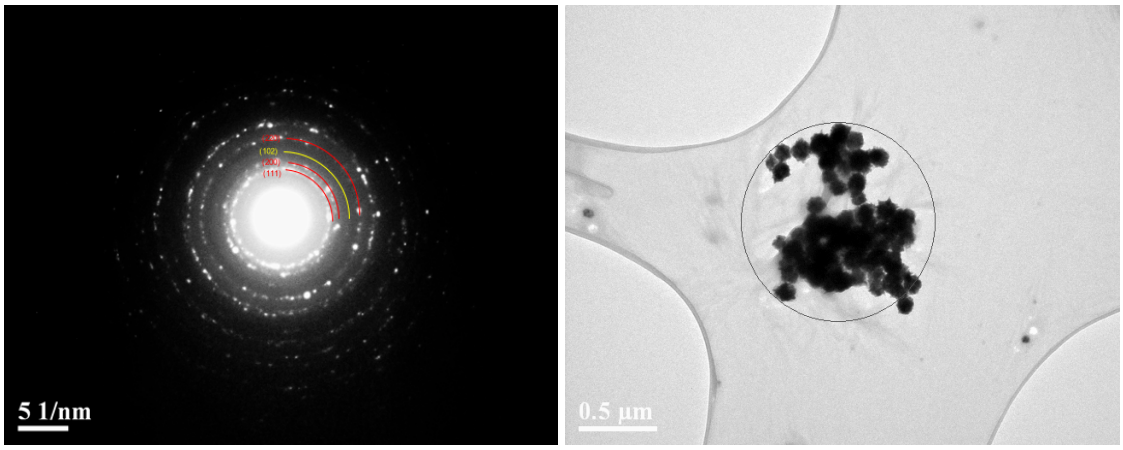

Figure 4.23: Diffraction pattern of Urchin Nickel without PVP after conversion.

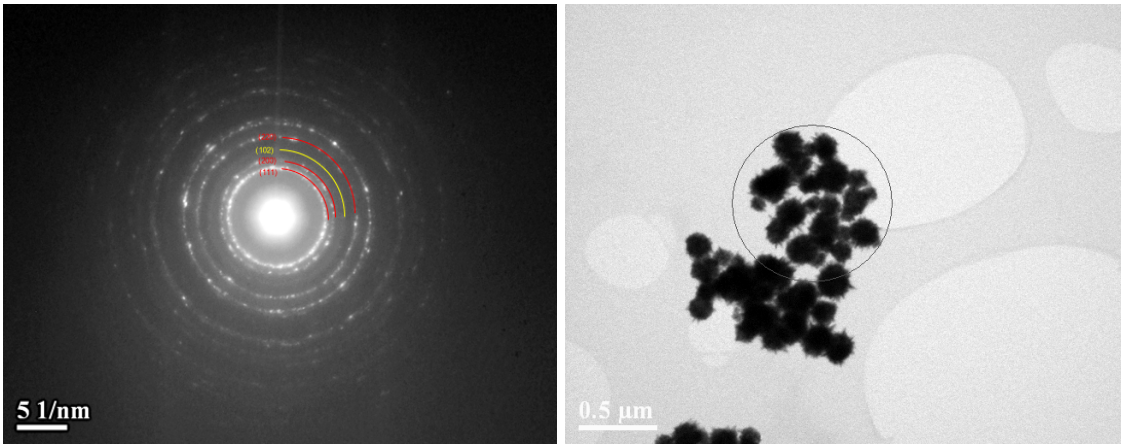

Figure 4.24: Diffraction pattern of Urchin Nickel with PVP after conversion.

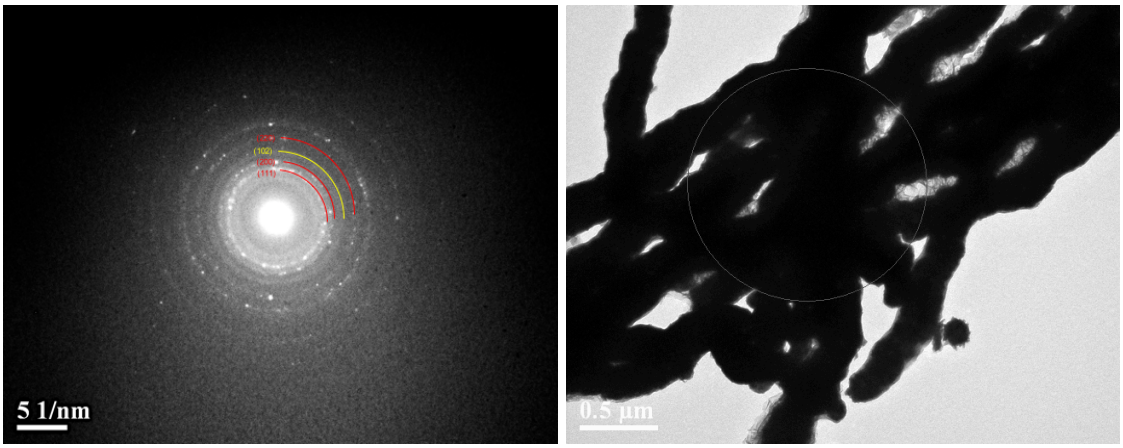

Figure 4.25: Diffraction pattern of Nickel Nanowire after conversion.

4.6.3. HRTEM Analysis and RGB Contrast

In this section, the exact location where nickel hydroxide forms on the particles is investigated. All of these samples are appropriate for HRTEM analyses in areas where the sample thickness is low or on the edges. Consequently, the locations where particles are converted to nickel hydroxide is shown in Fig. 4.26. After CV, triangular nickel has a layer of Ni-hydroxide on the surface of the particle. From the indexing of the interplanar spacing in high-resolution real space images the crystalline planes of Ni and β-Ni(OH)$_2$ have been indexed.

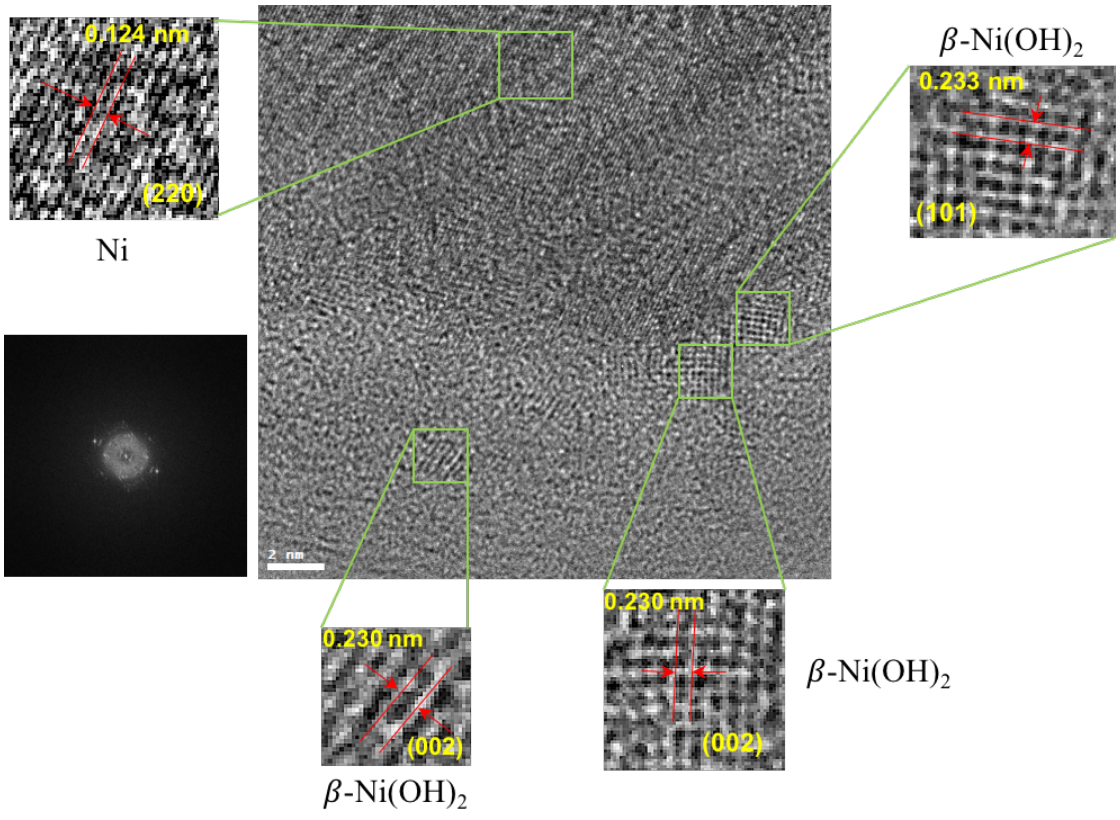

Figure 4.26: HRTEM of Triangular Nickel after conversion and FFT.

Because the Ni planes are detected more towards the inside of the particles, it can be stated that nickel hydroxide usually begins to grow on the surface of the particles, which is due to its contact with the electrolyte and surfaces can be converted more easily. For mapping of the spatial distribution of all phases, the RGB contrast helps to observe the locations of the beta-nickel hydroxide. As seen in Fig. 4.27, before the cyclic reaction, the whole structure is identified with the Ni planes (in Red) and no trace of nickel hydroxide is seen. However, after conversion, a significant amount of nickel hydroxide (Green regions) is present and this confirms the conversion. The same trend is shown in the RGB images (Fig. 4.28, 4.29, 4.30) for Urchin-like Nickel without PVP, Urchin-like Nickel with PVP and Nickel Nanowire, respectively.

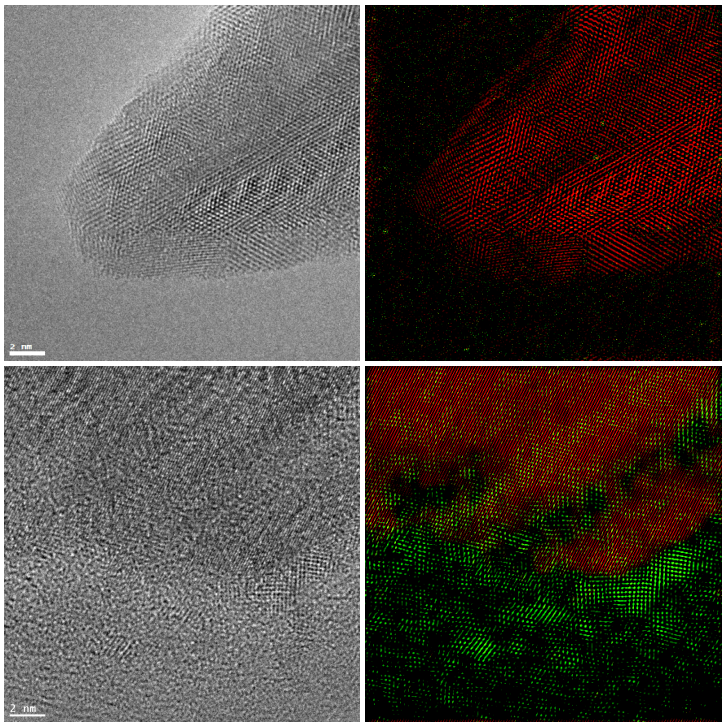

Figure 4.27: HRTEM and RGB images of Triangular Nickel before (Top) and after (Bottom) conversion.

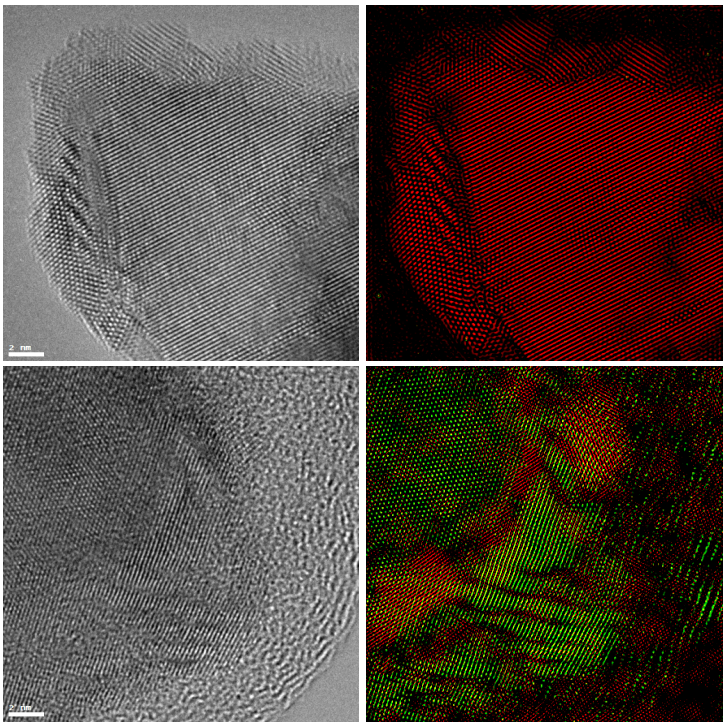

Figure 4.28: HRTEM and RGB images of Urchin Nickel without PVP before (Top) and after (Bottom) conversion.

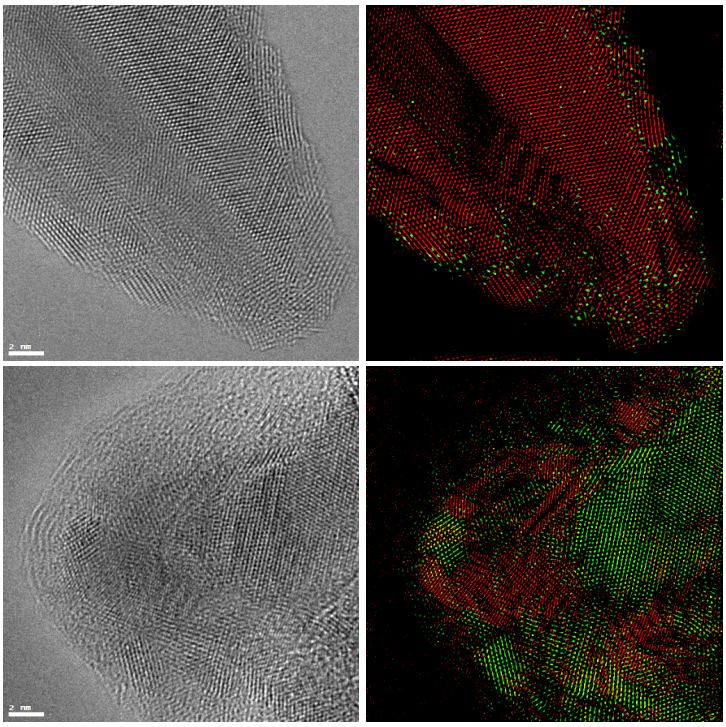

Figure 4.29: HRTEM and RGB images of Urchin Nickel with PVP before (Top) and after (Bottom) conversion.

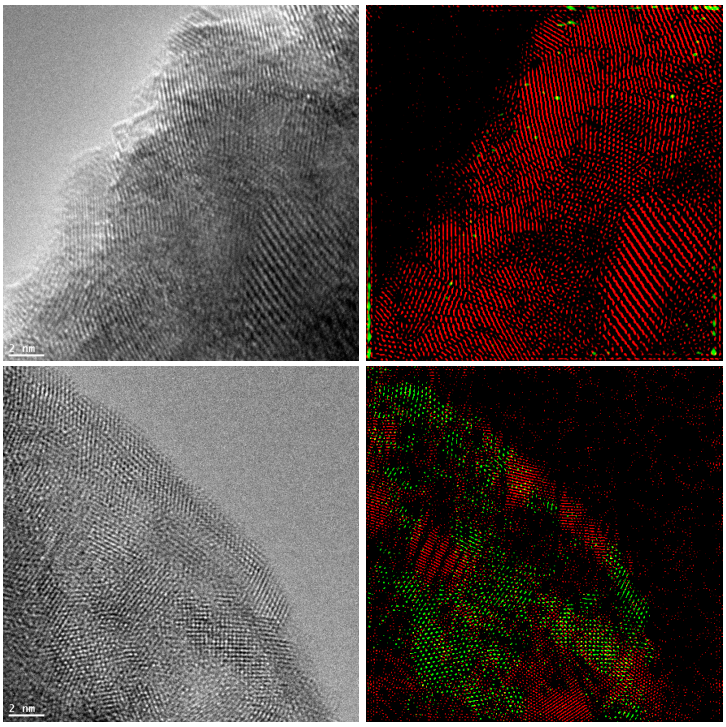

Figure 4.30: HRTEM and RGB images of Nickel Nanowire before (Top) and after (Bottom) conversion.

4.6.4. Tomography Analysis and 3D Modelling

The last test, which gives vital information, is Tomography. The purpose of this test is to examine the internal structure of nanoparticles. After preparing a tomogram file, the internal structure of nanoparticles, visualized slice by the slice, is obtained. As a result, this test shows not only the structure between particles but also inside of the particles. The 3D modelling from the structure is also accessible. This test has been performed on Triangular Nickel, Urchin Nickel without PVP and with PVP before and after CV. The number of tilted images is 65 (From -64 to +64 degrees, one image per 2 degrees increments). The total number of slices (or layers) reconstructed for the block of particles is 836 vertical slices.

Now, after the reconstruction by the software as discussed in the chapter 3, the tomogram file of these nanoparticles is generated. Fig. 4.31 shows slice number 400 in this block out of 836 slices. An impressive result of this reconstruction is that it is possible to visualize some porosity inside the particles. This type of structure can provide a means for the electrolyte to penetrate inside the agglomeration of particles although it would be necessary to assess if these pores are interconnected through a percolation network leading to the surface of the particles. The tomogram of the same sample (Fig. 4.31) after CV tests highlights again similar porosities. Another striking point in this characterization is the structure of particles. Each particle has limited contact with other particles (i.e. there is no dense packing as shown by the interparticle space in Fig. 4.31. This means that particles, due to their very irregular shape are not agglomerated with high density, and that a large interparticle active surface is available to react with the electrolyte.

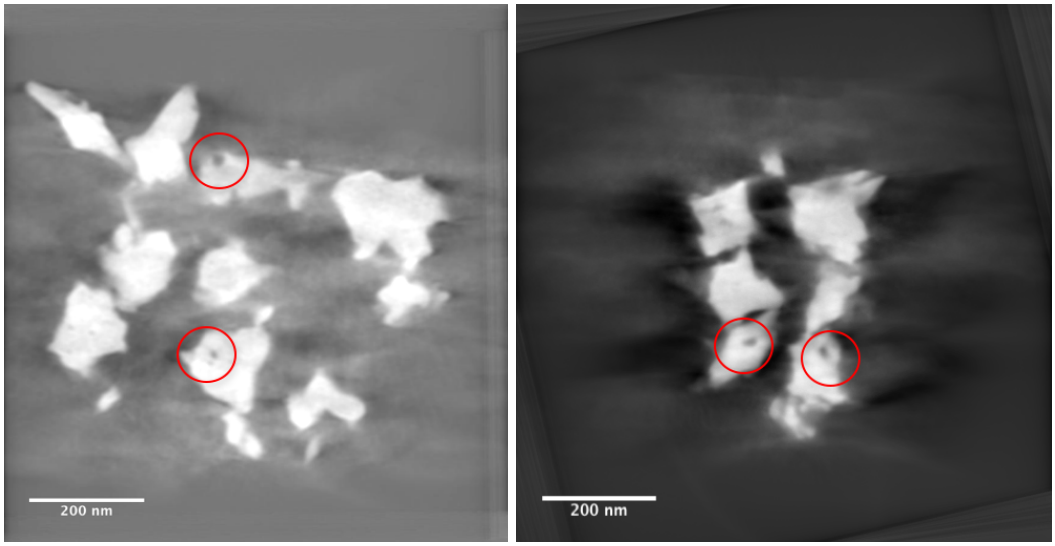

Figure 4.31: Slice No. 400 out of 836 of Tomogram before (Left) and after (Right) conversion.

Finally, using Visualization software such as Tomviz, the 3D modelling of the sample before conversion only is provided (Fig. 4.32). These reconstructions provide a very good visualization of the true shape of the particles which is much rougher than expected from simple visualization of 2D projections of the images from simple TEM imaging.

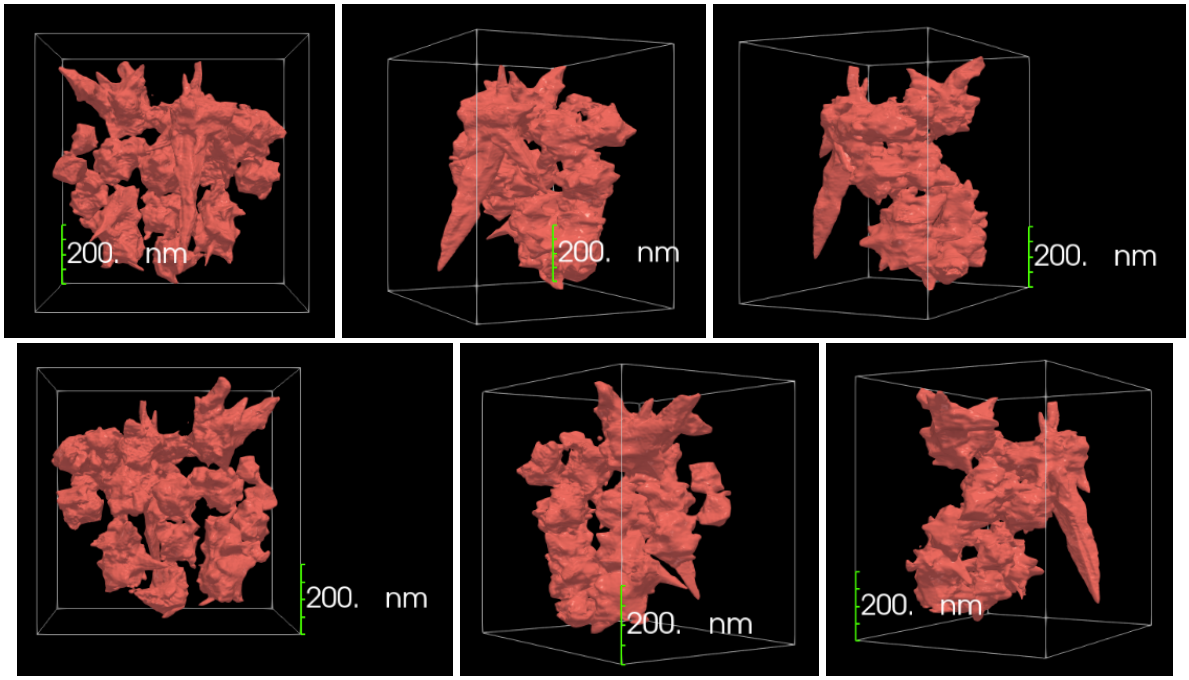

Figure 4.32: 3D modelling of Triangular Nickel before CV.

For Urchin-like Nickel, as seen in Fig. 4.33, porosity is even greater within the particles. The particle size is clearly more uniform than is observed for the Triangular Ni particles. From the internal porosity, this sample seems to be more suitable for transformation reactions. Fig. 4.34 displays 3D modeling of Urchin-like Nickel before conversion.

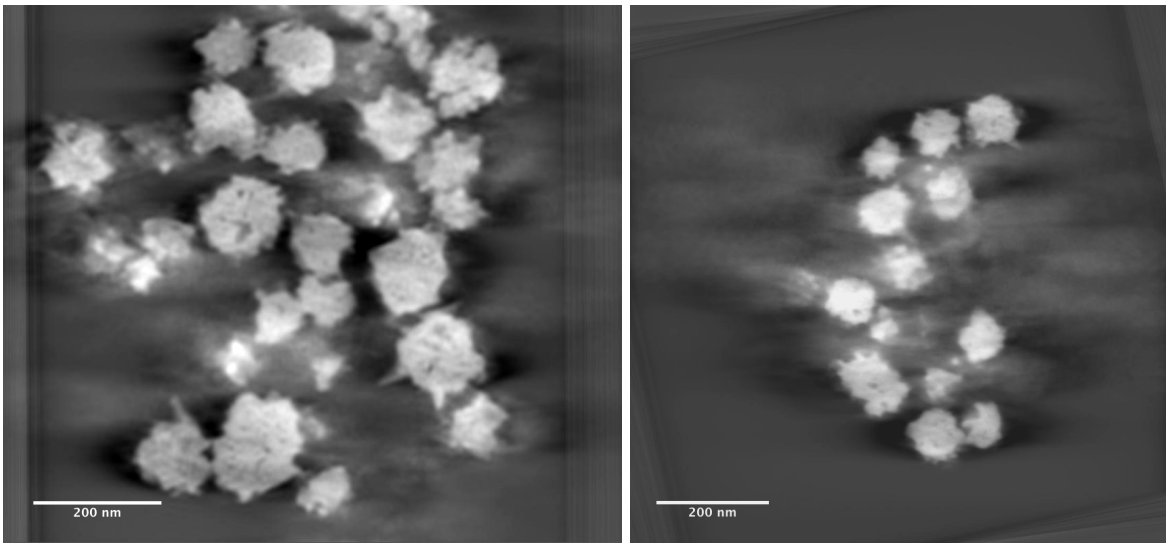

Figure 4.33: Slice No. 400 out of 836 of Tomogram before (Left) and after (Right) conversion.

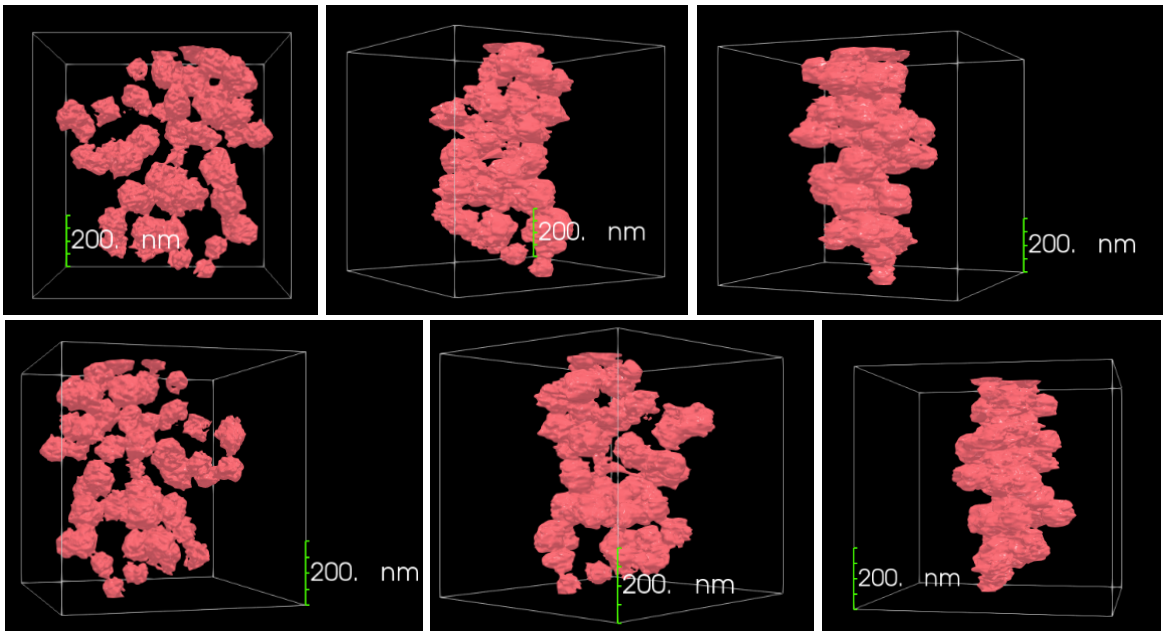

Figure 4.34: 3D modelling of Urchin Nickel without PVP before CV.

From these images, it is possible to see that the particles are much less irregular-shaped than the triangular Ni and that the surface is much smoother. Comparing the

samples before and after conversion, one cannot see very dramatic changes within the particles at the resolution allowed by the tomography reconstruction.

For the final sample, Urchin-like Nickel with PVP, there is also as much porosity inside the structure (Fig. 4.35). One of the reasons for this is the presence of polymer ligands in the synthesis of this type of nickel particles so that there is space between smaller particles making up the large individual Urchin-like Ni. The holes in this structure can potentially help to do conversion more quickly. Fig. 4.36 presents the 3D modelling before conversion which highlights the presence of sharp spikes all around the surface of the particles. These spikes would increase the surface area of the particles.

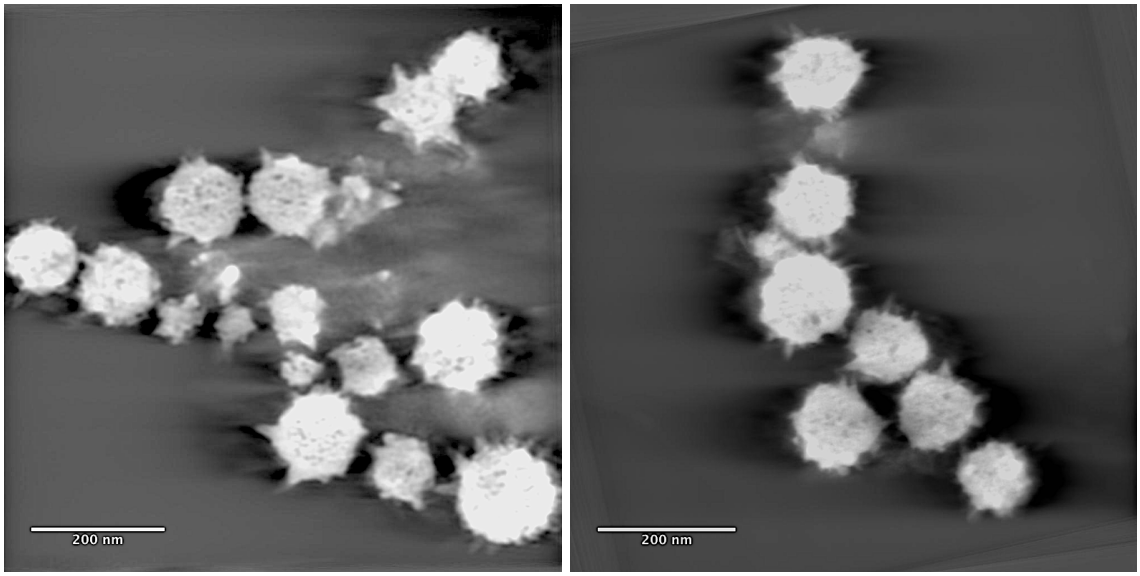

Figure 4.35: Slice No. 400 out of 836 of Urchin Nickel with PVP before (Left) and after (Right) CV.

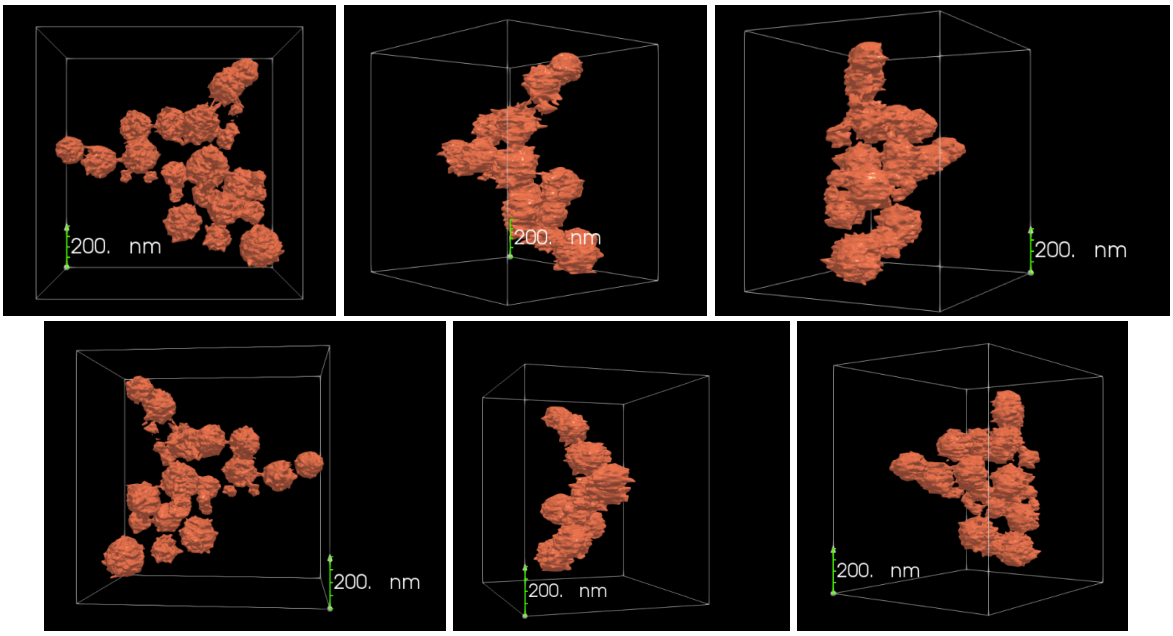

Figure 4.36: 3D modelling of Urchin Nickel with PVP before CV.

5. Conclusion and Future Work

As described in previous sections, the synthesis of the nickel hydroxide is done in two methods: one is the Direct method, leading to the presence of the alpha phase, and the other is the Indirect method generating the beta phase. Each of these methods has advantages and disadvantages. The phase that is usually required in alkaline reactions is the beta phase.

As an advantage of the alpha phase in the Direct method is that synthesis of this phase is easy and kinetically fast and is done with single reaction. Also, the whole structure is single-phase. The formation of microbubble allows the control of the nanostructure. Initially, the nickel hydroxide layer is formed, but after the cyclic reaction, the nanostructure can be transformed to the desired shape such as particles.

The advantage of the indirect method is the thermodynamic stability of the beta-phase, and also achieving β-$Ni(OH)_2$ directly. In this way, the nickel phase is easily converted to beta-nickel hydroxide, so various shapes of the nickel can be used in CV experiments. However, the main disadvantage of this method is that, after converting a volume of nickel to nickel hydroxide, a layer is formed on the surface. Consequently, this layer reduces the conversion rate, and remaining nickel in the core of particles cannot be converted. This causes the structure to have multi-phases nanoparticles. However, there are suggestions for solving this problem, including cyclic reactions in the higher number of cycles or synthesis of smaller nanoparticles with porosity inside to increase active surface area. We have also done experiments to study the structure

different particles prepared by our collaborators, the results show that nickel in different shapes is applicable to be converted to β-nickel hydroxide. Furthermore, porosity inside of the particles would be effective to improve conversion rate of nickel to nickel hydroxide due to penetration of electrolyte. This results in faster and easier conversion to avoid remaining nickel in the core of particles. Also, nanoscale particles with sharp edges cause less agglomeration and higher surface area.

As future work, the in-situ experiment can be done, and all conditions for characterization and modification of alpha and beta phases of nickel hydroxide are optimized. The in-situ test consists in creating an electrical circuit containing three electrodes is set up using a unique holder designed for electrochemical testing inside the electron microscope. In this case, special chips known as liquid cells are used, and glassy carbon is used as working electrode. Chips are placed on holder and electrolyte flows through very narrow pipes inside the holder. Moreover, all inputs and outputs of reactions are controlled by a potentiostat outside of TEM controlled by a computer. It must not have vacuum leakage during the experiments, and everything must be appropriately sealed. As a result, the synthesis of the nanoparticles can be observed simultaneously in real time. In future research, given the availability of several samples, in-situ experiments for the synthesis of nickel hydroxide in both Direct and Indirect methods and on pre-prepared samples by our collaborators could be carried out.

References

- Aert, S. V., Batenburg, K. J., Rossell, M. D., Erni, R., Tendeloo, G. V., doi:10.1038/nature09741.
- Alsabet, M., Grden, M., Jerkiewicz, G., Electrocatal (2011) 2:317–330.
- Argast, Anne, Tennis, Clarence F., III, 2004, A web resource for the study of alkali feldspars and perthitic textures using light microscopy, scanning electron microscopy and energy dispersive X-ray spectroscopy, Journal of Geoscience Education 52, no. 3, p. 213-217.
- Bard, A. J., Faulkner, L. R., Electrochemical methods Fundamentals and Applications, 1944.
- Bruker Nano GmbH, Berlin, Germany, info.bna@bruker.com, http://www.bruker.com/quantax-eds-for-sem.
- Budevski, E., Staikov, G., Lorenz, W. J., Electrochim. Acta, 2000, 45, 2559– 2574.
- Buseck, P. R., Cowley, J. M., Eyring, L., High-Resolution Transmission Electron Microscopy and Associated Techniques, Oxford University Press, 1988.
- Casella, I. G., Gatta, M., Anal. Chem. 72, 13, 2969-2975.
- Chen, J., Bradhurst, D. H., Dou, S. X., and Lui, H. K., J. Electrochem. Soc. 1999 volume 146, issue 10, 3606-3612.
- Chen, J., Bradhurst, D. H., Dou, S. X., Liu, H. K., *Journal of The Electrochemical Society,* 146 (10) 3606-3612 (1999).
- Dai, J., Li, S. F.Y., Xiao, T. D., Wang, D. M., Reisner, D. E., Journal of Power Sources 89 (2000) 40–45.
- Dehai, P., Review on ω Phase in Body-Centered Cubic Metals and Alloys. Acta Metallurgica Sinica (English Letters), 2014, 27(1): 1-11.

- Denuault, G., Mirkin, M. V., Bard, A. J., J. Electroanal. Chem., 308 (1991) 27-38.
- Dudin, P. V. Unwin, P. R., Macpherson, J. V., J. Phys. Chem. C, 2010, 114 (31), pp 13241–13248.
- Evans, J. E., Jungjohann, K. L., Browning, N. D., Arslan, I., Nano Lett. 2011, 11, 2809–2813.
- Fisher, A. C. "Electrochemistry Teaching Notes" in the website of the Department of Chemical Engineering and Biotechnology, University of Cambridge, 2010. http://www.ceb.cam.ac.uk/research/groups/rg-eme/teaching-notes.
- Freitas, M.B.J.G., Journal of Power Sources 93 (2001) 163±173.
- Gamry Instruments, Inc., Revision 6.0, 2012, 988-00006.
- Gibson, J.M., High Resolution Transmission Electron Microscopy, 1991, https://doi.org/10.1557/S0883769400057377.
- Goodhew, P., Humphreys, J., Beanland, R. (2000). Electron Microscopy and Analysis. London: CRC Press.
- Hall, D. S., Lockwood, D. J., Bock, C., MacDougall, B. R., Proc. R. Soc. A 471: 20140792.
- Hall, D. S., Lockwood, D. J., Poirier, S., Bock, C., MacDougall, B. R., J. Phys. Chem. A 2012, 116, 6771−6784.
- Hofmeister, H., Huisken, F., Kohn, B., Alexandrescu, R., Cojocaru, S., Crunteanu, A., Morjan, I., Diamandescu, L., Appl. Phys. A 72, 7–11 (2001) / Digital Object Identifier (DOI) 10.1007/s003390000599.
- Hu, W.K., Noréus, D., Chem. Mater. **2003,** 15, 974-978.
- Hutton, L. A., Vidotti, M., Patel, A. N., Newton, M. E., Unwin, P. R., Macpherson, J. V., *J. Phys. Chem. C,* 2011, 115 (5), pp 1649–1658.
- Kissinger, P. T., Heineman, W. R., Journal of Chemical Educations, Volume 60 Number 9, September 1983, 702-706.

- Lertviriyapaisan, S., Tantavichet, N., International journal of hydrogen energy 35 (2010) 10464 e10471.
- Lu, X., Zhao, C., 2015, Nature Communications | 6:6616 | DOI: 10.1038/ncomms7616.
- Machado, S. A. S., Avaca, L. A., Electrochimica Acta, Vol. 39. No. 10. pp. 1385 - 1391. 1994.
- Messaoudi, C., Boudier, T., Sorzano, C. O. S., and Marco, S., TomoJ: tomography software for three-dimensional reconstruction in transmission electron microscopy. BioMed Central BioInformatics Ltd. 2007, 8-288.
- Milne, J. L.S., Subramaniam, S., Cryo-electron tomography of bacteria: progress, challenges and future prospects, Nature Reviews Microbiology volume7, pages666–675 (2009), doi:10.1038/nrmicro2183.
- Nicholson, R. S., Chemistry Department, Michigan State University, East Lansing, Mich. VOL. 37, NO. 11, October 1965.
- Rajamathi, M., Kamath, P. V., Seshadri, R., J. Mater. Chem., 2000, 10, 503±506.
- Reier, T., Oezaslan, M., Strasser, P., ACS Catal. 2012, 2, 1765−1772.
- Rocha, M. A., Winnischofer, H., Araki, K., Anaissi, F. J., Toma, H. E., Journal of Nanoscience and Nanotechnology Vol. 11, 3985–3996, 2011.
- Roussel, L. Y., Stokes, D. J., Gestmann, I., Darus, M., Young, R. J., Proc. of SPIE Vol. 7378 73780W-1.
- Sharel P. E., Liu, Danqing, Lazenby, Robert A., Sloan, Jeremy, Vidotti, Marcio, Unwin, Patrick R. and Macpherson, Julie V, J. Phys. Chem. C 2016, 120, 16059−16068.
- Sorzano, C. O. S., Messaoudi, C., Eibauer, M., Bilbao-Castro, JR., Hegerl, R., Nickell, S., Marco and JM Carazo: Marker-Free Image Registration of Electron Tomography Tilt-Series. BioMed Central BioInformatics Ltd. 2009, 10:124.
- Steven, A. C., Aebi, U., cryo-electron tomography of intact cells, TRENDS in Cell Biology Vol.13 No.3 March 2003.

- Stroppa, D. G., Dalmaschio, C. J., Houben, L., Barthel, J., Montoro, L. A., Leite, E. R., Ramirez, A. J., Chem. Eur. J. 2014, 20, 6288 – 6293.
- Sutherland, B., Nickel 04/07/2009, http://www.thecanadianencyclopedia.ca/en/article/nickel/.
- Thanh, N. T. K., Maclean, N., Mahiddine, S., *Chem. Rev.*, 2014, 114 (15), pp 7610–7630.
- Vidotti, M., Salvador, R. P., Torresi, S. I. C., Ultrasonics Sonochemistry 16 (2009) 35–40.
- Weyland, M., Midgley, P. A., Electron Tomography, ISSN:1369 7021 © Elsevier Ltd 2004.
- Williams D.B., Carter C.B. (1996) The Transmission Electron Microscope. In: Transmission Electron Microscopy. Springer, Boston, MA.
- Wu, M.S., Huang, K.C., Chem. Commun., 2011, 47, 12122–12124.
- Zhao, D.D., Bao, S.J., Zhou, W.J., Li, H.L., Electrochemistry Communications 9 (2007) 869–874.